Tunable vegetable oil/silica hybrid microparticles for poorly water-soluble drug delivery

Koceïla Doufène, Vincent Lapinte, Philippe Gaveau, Gautier Félix, Thomas Cacciaguerra, Joel Chopineau, Jean-Jacques Robin, Jean-Marie Devoisselle, Anne Aubert-Pouëssel

Tunable vegetable oil / silica hybrid microparticles for poorly water-soluble drug delivery

Koceïla Doufène, Vincent Lapinte, Philippe Gaveau, Gautier Félix, Thomas Cacciaguerra, Joël Chopineau, Jean-Jacques Robin, Jean-Marie Devoisselle, Anne Aubert-Pouëssel*.

ICGM, Univ Montpellier, CNRS, ENSCM, Montpellier, France.

*** Corresponding Author Email Address**: anne.aubert@umontpellier.fr

ABSTRACT

To encapsulate and deliver poorly water-soluble drugs, castor oil/silica hybrid microparticles (HMP)s were synthesized. Green chemistries were used to silylate the oil and further cross-link it into solid microparticles by sol-gel reaction. Silylated castor oils (ICO)s at various silylation ratios were prepared and allowed the solubilization of ibuprofen at several concentrations up to 16 wt%. The HMPs were formulated by ThermoStabilized Emulsion (TSE) process which permits to “freeze” the oil-in-water emulsion while the sol-gel reaction occurs.

The hybrid mineral / organic composition and the morphology (spherical shape and micrometric size) of these HMPs were determined by complementary technics (SEM, TGA, EDX, ^{29}Si NMR and FTIR spectroscopies).

The HMPs reached a good ibuprofen loading efficiency regardless to the formulation used while the release kinetics in simulated oral administration exhibited a tunable release during 3 hours according to the silylation ratio. The ibuprofen rate also influenced its own amorphous or crystalline character within the HMPs. For subcutaneous conditions, ibuprofen release took place over 15 days. Finally, biodegradability assays in simulated digestion medium suggested a surface-limited hydrolysis of the particles and cytocompatibility studies on NIH-3T3 and Caco-2 cells demonstrated an excellent cellular viability.

ABBREVIATIONS:

API: Active Pharmaceutical Ingredient = drug; CO: Castor Oil; EDX: Energy Dispersive X-ray; (F)FA: (Free) Fatty Acid; FTIR: Fourier Transform Infrared; HMP: Hybrid Microparticle; ICO: silylated castor oil; LBDDS: Lipid-Based Drug Delivery System; NMR: Nuclear Magnetic Resonance; O/W: Oil-in-Water; SEM: Scanning Electronic Microscopy; SGF: Simulated Gastric Fluid; SIF: Simulated Intestinal Fluid; TG: Triglyceride; TGA: Thermogravimetric Analysis; TSE: Thermostabilized Emulsion, wt%: weight percentage.

KEYWORDS:

Vegetable oil; Sol-gel; Silica; Hybrid microparticle; Drug delivery system; Poorly water-soluble drug.

ARTICLE

1. Introduction

The continuous improvement of health conditions over the last decades increased the incidence of so-called "ageing" and "civilization" diseases such as diabetes, hypertension, neurological degenerations and cancers. The pharmaceutical research and the development of Active Pharmaceutical Ingredients (API)s are therefore in great demand. However, the vast majority of these APIs have solubility issues and their “drug-like” profiles are compromised during early stages of the development (Kruse et al., 2008). Several formulations have been studied to overcome this limit. Lipid-based drug delivery systems (LBDDS) dominated these formulations owing to their high solvation capacity on poorly water-soluble APIs. The composition of LBDDS varied according widely to its use, ranging from simple lipids such as fatty acids (FA)s and triglycerides (TG)s to more complex systems like self micro- and nano-emulsifying LBDDS which contain phospholipids, surfactants, co-surfactants and co-solvents in addition to FA and TG. Liposomes were predominant as LBDDS for the parenteral administration and many formulations were commercialized such as Ambisome® (amphotericin B) or Doxil® (doxorubicin) (Chen and Yazdi, 2013). In addition, solid lipid particles showed a high potential of drug entrapment and delivery via parenteral route. Indeed a wide variety of chemotoxics (paclitaxel, camptothecin), corticoids (hydrocortisone, prednisolone) and anesthetics (tetracaine, etomidate) was loaded into solid lipid nanoparticles and their preclinical trials were promising (Wissing et al., 2004). For the oral administration, the Lipid Formulation Classification System divided the LBDDS into four types depending on their composition and their behavior in the gastrointestinal gut (Pouton and Porter, 2008). The type I consists in digestible oils without surfactants whereas the type II contains water-insoluble ones. The type III is made of oils, surfactants and cosolvants. It is subdivided into IIIA, which is predominantly made of oil, and IIIB, which contains more water-soluble components. The type IV is free of oils and contains only self-assembling surfactants and cosolvants, which makes it unlikely digestible. Despite the interest of LBDDS, they require large quantities of organic solvents that represent a non-valuable industrial input and required additional purification of the final product. On the other hand, many complex approaches were considered to solidify these LBDDS in order to improve their pharmacotechnical properties and enhance their stability (Kalepu et al., 2013). For example,

the spray-congealing consists in a molten lipid sprayed into a cooling chamber to form cooled solid particles (e.g., diclofenac in stearoylpolyoxylglycerides "Gelucire® 50/13") whereas the spray-drying consists on a solution of drug and lipid excipients sprayed inside an atomizing chamber (e.g., glibenclamide in silicon dioxide and Gelucire®), to form spherical solid particles in both cases. Carbone dioxide in supercritical physical state was also involved in the solubilization and reprecipitation of lipid excipients for drug coatings (e.g., carbamazepine in vitamin E, TPGS and Gelucire® 44/14). Unfortunately, these processes remain highly energy-intensive and require complex equipments.

To circumvent the use of organic solvents and complex manufacturing processes, an original approach combining vegetable oil recovery, eco-friendly chemistry and simple pharmacotechnology process was investigated. As firstly demonstrated by Gallon et al. (Gallon et al., 2017), bio-based hybrid microparticles for drug delivery have already been synthesized by this technology coupling castor oil silylation and a thermostabilized emulsion (TSE) process. Resulting microdroplets of silylated castor oil (ICO) were cross-linked by a sol-gel reaction inducing the solidification of the organic / inorganic hybrid microparticles (HMP)s at ambient temperature. Preliminary tests were carried out on the microparticles to optimize their preparation process, to characterize their structure and to assess their ability to entrap ibuprofen as model of poorly water-soluble API.

Herein, the HMPs drug delivery kinetics were investigated using several castor oil-based formulations that differ either in the organic/inorganic ratio of the ICO or the ibuprofen loading rate. The TSE process was optimized to improve the biocompatibility of the HMPs for a pharmaceutical application using a catalyst approved by the US Food and Drug Administration (US-FDA). Comprehensive and multi-scale physicochemical studies were achieved on synthesized particles regarding to their shape and size, condensation degree, organic/inorganic composition and atomic distribution. We designed several types of ibuprofen-loaded HMPs, and monitored their release kinetics in various simulated media. The drug release kinetics were characterized by mathematical modeling to prove the influence of the matrices on the API diffusion. To conclude this screening, the hybrid microparticles degradability in simulated digestion medium was studied and their biocompatibility assessed on NIH-3T3 (fibroblasts) and Caco-2 cells (enterocytes-like cells).

2. Materials and methods

2.1. Materials

Pharmaceutical grade castor oil (CO; 934 g·mol^{-1}) was purchased from Cooper Pharmaceutique. (3-Isocyanatopropyl)triethoxysilane (IPTES; 247.3 g·mol^{-1}), stannous octoate (SnOct; 405.1 g·mol^{-1}), κ-carrageenan, ibuprofen (206.3 g·mol^{-1}) and flurbiprofen (244.3 g·mol^{-1}), bile extract porcine, pancreatin from porcine pancreas (4 × USP specifications) and polysorbate 80 (PS80; Tween® 80) were purchased from Sigma-Aldrich and Soybean phospholipids (S100) from Lipoid. Solvents such as acetonitrile HPLC plus Gradient (ACN), acetic acid, methanol (MeOH) and salts such as sodium chloride (NaCl), sodium phosphate dibasic (Na_2HPO_4, $12H_2O$) and potassium phosphate monobasic (KH_2PO_4) were also supplied by Sigma-Aldrich, while potassium chloride (KCl) was provided by Panreac Quimica, calcium chloride ($CaCl_2$, $2H_2O$) by Merck and sodium acetate (CH_3COONa, $3H_2O$) by VWR chemicals.

2.2. Silylation of the castor oil

Castor oil, which contains 90 % of ricinoleic acid, was functionalized with IPTES for 72 hours at 60 °C under nitrogen atmosphere, following a solvent- and catalyst-free process (Fig. 1). Four ratios of silylation X_R between IPTES and CO were established: 1.05, 0.8, 0.6 and 0.4. These x_R corresponded to the percentage of CO hydroxyl groups related to the isocyanate groups of IPTES (1.05 = 100 % with 5 % excess of free IPTES; 0.8 = 80 %; 0.6 = 60 % and 0.4 = 40 %). The silylated castor oils (ICO)s were aimed to synthetize several types of HMPs, designated with the same x_R. The completion of the reaction was checked by ATR-IR spectroscopy with a Spectrum 100 from Perkin Elmer (Li et al., 2016).

2.3. Formulation of the hybrid microparticles

As described in our previous paper (Gallon et al., 2017), HMPs were formulated according to an original process (Fig. 2) based on a thermostabilized oil-in-water emulsion (TSE). The TSE process was optimized for a pharmaceutical application by the use of SnOct, a US-FDA approved catalyst for food packaging (Department of Health and Human Services, 2018) and biomedical devices (Niemeyer and Mirkin, 2007, p. 296), instead of Dibutyltin dilaurate (DBTDL). The oil phase was composed of ICO with 1 % of SnOct ± ibuprofen dissolved at several rates ranging from 4 wt% up to 16 wt% into the ICO, prior to its formulation. Thus each formulation differed either by the ICO amount (0.4, 0.6, 0.8, 1.05) or by the rate of ibuprofen dissolved (4, 8, 12 and 16 wt%). The aqueous phase consisted of an acetate

aqueous buffer (2N) at pH=2.8 with 0.5 wt% of κ-carrageenan (thermogelling agent) and 0.3 wt% of KCl (thermogel stabilizer (Mangione et al., 2005)). The O/W emulsion was formed at 60 °C with a T 18 digital Ultraturrax® (IKA) at 9000 rpm for 2 min, then a thermal shift (from 60 °C to 4 °C) was applied in order to gel the aqueous phase and stabilize the oil droplets in which the sol-gel reaction occurred at 25 °C. The acetic acid within the acetate buffer leads to a better hydrolysis of ethoxysilanes while SnOct improves the network condensation (Brinker, 1988; Shi et al., 2012). This combination of catalyst (SnOct) and co-catalyst (acetic acid) permitted to accelerate the sol-gel reaction down to 8 days. Once HMPs were solidified, the gel was disrupted by heating to 60 °C. The HMPs were washed with distilled water, separated by centrifugation at 4000 rpm for 6 min and freeze-dried (Heto Powerdry® LL3000, Thermo Fisher Scientific). After recovery, preparation yields **η** were calculated by dividing the weight of dried particles by the initial mixture weight (ICO + catalyst ± API) (eq. 1)

$$\boldsymbol{\eta} = \frac{\textbf{Weight of recovered particles}}{\textbf{initial oil phase weight}} \qquad \textbf{(1)}$$

2.4. Characterization of the hybrid microparticles

2.4.1.Physicochemical characterization

Firstly, the HMP morphologies were analyzed both by optical microscopy (Axiolab® equipped with AxioCam® ERc 5s model, Zeiss) and scanning electron microscopy (SEM, Hitachi S4800 high resolution). HMPs size measurements were assessed by laser diffraction (Mastersizer® 2000, Malvern instruments) in a Hydro 2000SM dispersion unit with absolute ethanol as a dispersion medium. This technique allowed to draw volume size distributions of the HMPs, to determine Volume Median Diameters[*] (VMD) and to deduct Moment means (Rawle, 2018). The volume moment mean D[4,3] [†] was interesting in our case because it takes into account the spherical volume of HMPs. For the entrapped API, the distance to reach the surface depends indeed on this volume. As well, surface area moment mean D[3,2] [‡] is even of interest considering that API release is modulated by the extent of HMPs surface area. A Kruskal-Wallis test in Anastats® software was used to compare the results and $P < 0.05$ value was considered statistically significant.

[*] The Volume Median Diameter refers to the midpoint particle size where half of the total volume is in HMP smaller, and half in HMP larger.

[†] $\mathrm{D}[4,3] = \frac{\Sigma\, d^4}{\Sigma\, d^3}$

[‡] $\mathrm{D}[3,2] = \frac{\Sigma\, d^3}{\Sigma\, d^2}$

The sol-gel cross-linking (hydrolysis and condensation) was monitored with IR-ATR spectroscopy (Spectrum 100, Perkin Elmer) and the condensation was quantified by solid state ^{29}Si-NMR (Varian VNMRS 400 MHz [9.4T] NMR spectrometer, with a 7.5 mm Varian T3 HX MAS probe spinning at 5 kHz). Two sequences of NMR at Magic Angle Spinning (MAS) were assessed: a Cross Polarization (CP-MAS) and a Single Pulse sequence (SP-MAS) with ^{1}H decoupling. CP-MAS experiments were performed with a 1.5 ms contact time and a recycle delay of 5 s in order to measure chemical shifts corresponding to silica fraction units present in each sample. For the quantitative determination of identified silica fraction units, SP-MAS experiments were carried out using a 2µs 30° pulse and a recycle delay of 60 seconds. Spectra were accumulated overnight in order to increase the signal-to-noise ratio. Dmfit program (Massiot et al., 2002) was used to fit peaks and areas under curves were integrated for each unit and expressed in percent.

In order to determine the atomic composition and the API disposition within particles, flurbiprofen-loaded HMPs were studied by energy dispersive X-ray (EDX, FEI Quanta 200 FEG SEM). One micrometer cube was analyzed at each dot and backscattered-electrons were recorded (Oxford Instruments, X-Max^{N} Silicon Drift Detector). Flurbiprofen as well as ibuprofen is a nonsteroidal anti-inflammatory drug belonging to aryl carboxylic family (Fig. A.1). It was selected for its fluorine atom that can be mapped by EDX within HMPs. The mineral part of HMPs was also estimated by thermogravimetric analysis (TGA; STA 6000, PerkinElmer) from 25 to 900 °C at 10 °C.min^{-1} under airflow.

2.4.2.Pharmaceutical characterization

The loading efficiencies of ibuprofen-loaded HMPs at 4, 8, 12 and 16 wt% were determined by dispersing 50 mg of each formulation in 10 mL of methanol overnight, prior to an HPLC dosage (LC-2010HT Shimadzu, static phase: C18 Protonsil® column from Bischoff, mobile phase: acetonitrile/ 0.5 % acetic acid solution, 65/35 v/v). Encapsulation yields were calculated using eq. 2:

$$\textbf{Encapsulation Yield} = \textbf{Loading rate after formulation} \times \eta' \qquad \textbf{(2)}$$

Where η' is the corrected preparation yield (taking into account the hydroxyethyl loss – see results).

The crystalline state of the entrapped ibuprofen was also checked. Two analyses were done: X-Ray powder Diffraction (XRD; Bruker D8 advance generator equipped with copper tube and 1d LYNXEYE detector, λ= 1,5406 Å, acquisition from 5 to 40° of 2Θ angle) to detect ibuprofen crystals and Differential Scanning Calorimetry (DSC; DSC4000,PerkinElmer, sample heated from 20 to 95 °C at 10 °C.min^{-1} under 50 mL.min^{-1} of nitrogen flow) to track the melting point of API crystals within the matrix.

Furthermore, *in vitro* releases were assessed from ibuprofen-loaded HMPs using flow-through cell apparatus (Sotax CE1) according to the United States Pharmacopoeia (USP) IV specifications for poorly water soluble APIs dissolution (Paprskářová et al., 2016). Three protocols were established for the purpose, depending on the buffer system used: in protocol **(1),** 25 mL of Simulated Gastric Fluid (SGF, hydrochloride solution containing 0.1 wt% PS80, pH = 1.2 at 37 °C) were used as a release medium for 30 minutes, then 25 mL of an intermediate solution where added in order to reach 50 mL of a Simulated Intestinal Fluid (SIF, 50 mM of phosphate buffer containing 0.1 wt% of PS80, pH = 6.8 at 37 °C) whereas in protocols **(2)** and **(3)**, 50 mL of media were directly used as follows **(2):** SIF, 50 mM of phosphate buffer containing 0.1 % of PS80, pH = 6.8 at 37 °C and **(3)**: 12 mM of phosphate buffer without PS80, pH = 7.4 at 37 °C (Stippler et al., 2004). PS80 is a hydrophilic surfactant used here at 0.1 wt% to decrease the surface tension of release media down to 42 mN·m^{-1}. The low surface tensions of gastric juice reported between 35 and 45 mN·m^{-1} (Efentakis and Dressman, 1998; Finholt and Solvang, 1968) and the intestinal fluid around 50 mN·m^{-1} (Klein, 2010) were thus simulated, ensuring an optimal dispersion and wettability of HMPs. The system was then connected in closed loop through powder cells containing 50 mg of microparticles. 1 mL samples were collected at defined times prior to an HPLC dosage and 1 mL of fresh medium was added after each sampling to maintain the volume constant.

A mathematical model for 4 wt% ibuprofen-loaded HMPs releases in Simulated Intestinal Fluid (SIF) was established and described in Appendix B.

2.4.3.Biological characterization

Biodegradability and biocompatibility of HMPs were assessed. Biodegradability assays were achieved on the particles following a simulated digestion protocol. An AT7 smart Dissolution Apparatus from Sotax (USP II) was used as an incubation system: 500 mg of microparticles were dispersed in 50 mL of a pre-digestion medium at 37 °C, with continuous stirring (see

Table A.1 for composition). As a reference, 500 mg of CO were emulsified in 50 mL of pre-digestion medium following the same protocol as used for the HMPs formulation (9000 rpm for 2 min with T 18 digital Ultraturrax®). The lipase was then added to initiate the digestion. 1 mL samples were collected at defined times and their pHs were consecutively measured using a SevenCompact pH-meter equipped with an Inlab® Micro sensor (Mettler Toledo). 1mL of an aqueous solution of $CaCl_2$ ($[Ca^{2+}]$ = 36mM) was added in each medium in order to maintain media volumes constant while the Ca^{2+} continuously precipitate the Free Fatty Acids (FFAs) liberated during the digestion (Zangenberg et al., 2001). These FFAs, composed at 90 % of ricinoleic acid (pKa= 4.74), 4 % of linoleic acid (pKa=4.77) and 3 % of oleic acid (pKa=5.02), were able to exhibit their acidities at pH of the medium (pH=6.8). Thus, a pH drop versus time curve was drawn for each sample in order to monitor the digestion (Mosgaard et al., 2015).

On the other hand, cytotoxicity studies of the HMPs were conducted according to the ISO 10993 norm. The cytocompatibility of the particles was assessed by following the viability of two cell lines: Caco-2/TC7 enterocytes and NIH-3T3 fibroblasts. These cell lines were selected to simulate an intestinal environment for an oral administration of HMPs and a dermal environment for a subcutaneous administration, respectively. Cells were treated with microparticles extracts using a CellTiter 96® AQ cell proliferation assay (Promega) composed of a tetrazolium compound (3-(4,5-dimethylthiazol-2-yl)-5-(3-carboxymethoxyphenyl)-2-(4-sulfophenyl)-2H-tetrazolium, inner salt: MTS) and an electron coupling reagent (phenazine methosulfate: PMS). The cells were seeded at 5000/well density into a 96-well culture dish plate containing 200 µL/well of a culture medium (Dulbecco's Modified Eagle Medium: DMEM) and permitted to adhere at 37 °C and 5 % CO_2 for 24 h. Subsequently, they were treated with various samples (particle suspensions: 0.1, 1 or 10 $mgmL^{-1}$, incubated 2 days at 37 °C). After 24 h of exposure, 20 µL of a mixture MTS-PMS was added according to the manufacturer instructions for 4 h reaction with the cells. The assay plate was read at 490 nm using a microplate reader (Multiskan Go, Thermo Fisher Scientific). The absorbance of the untreated cells (control group) corresponded to the 100 %.

3. Results and discussion

3.1. Castor oil functionalization and hybrid microparticles formulation

Castor oil was silylated with IPTES in solvent- and catalyst-free conditions corresponding to the first stage of the HMPs preparation. For the four ratios X_R studied, the silylation reaction was followed by IR-ATR spectroscopy (Fig. 3) wherein two chemical groups could be monitored: i) the disappearance of the isocyanate group labeling the IPTES (Socrates, 2010), which exhibits an asymmetric stretching vibration band at 2270 cm^{-1}; ii) the appearance of urethane group characterized by three vibration bands: (a) an amid-I band at 1720 cm^{-1} corresponding to the C=O stretching vibration; (b) an amid-II band at 1700 cm^{-1} corresponding to the N-H bending vibration (these two bands were shouldered by the C=O vibration band of the ricinolein ester function) and (c) a band at 1240 cm^{-1} resulting from interaction between C-N stretching and N-H bending (Cannon, 1976; Silverstein et al., 2005, p. 100). However, the disappearance of ricinolein hydroxyl groups cannot be confidently monitored because of the overlapping between O-H and N-H stretching bands at adjacent frequencies (around 3400-3500 cm^{-1}).

The completion of hydroxy-isocyanate reaction between the IPTES and the ricinolein was attested for the four silylation ratios. In all cases, isocyanate group transmittance (2270 cm^{-1}) was proportional to the IPTES engaged in each reaction. They were minimal at t=0 and increased to a 100 % transmittance at t_{final}=72 hours. By contrast, the urethane group transmittances (1720, 1700 cm^{-1} and 1240 cm^{-1}) decreased during the same period. Four ICOs with high purity where thus formed exhibiting an oily aspect and transparent to yellowish appearances. The physicochemical properties of these ICOs (Table 1) were consistent with their chemical structures: the silylation of the CO increased its molecular weight (from 932 to 1600 $g \cdot mol^{-1}$ for the higher X_R), which induced an increase of the viscosity (from 661 to 961 mPa·s) and density (from 0.907 to 0.999). During the HMPs formulation, the viscosity is an important parameter and difference in ICOs viscosities could affect emulsion properties.

The second stage of HMPs preparation consists in their formulation by a TSE process in aqueous medium (Fig. 2). To calculate relevant preparation yields, hydroxyethyl moieties released during hydrolysis (as described below) had to be taken into account. Therefore, assuming that the hydrolysis of ethoxysilanes was complete in our case, corrected preparation

yields **η'** were calculated (Table 2) and displayed excellent values ranging from 87.4 to 95.3 %. The robustness of the process was thus proven since there is no influence of the silylation ratio on the preparation yield.

3.2. Physicochemical characterization of hybrid microparticles

Hybrid microparticles were spherically shaped through the emulsification step of TSE process. According to ICO amount, various HMP surface states were observed by SEM: for HMPs 1.05, rough and irregular surface (Fig. 4-A) whereas more regular and smooth textures were exhibited at the surface of HMPs 0.8 to 0.4 (Fig. 4-B to D). However, some broken particles were noticed on the overview of HMP 0.4 (Fig. 4-D). It may be explained by the low X_R of these particles, which leads to less potential siloxane bonds and results in a weaker cohesion of these objects. A matrix structure was also uncovered on cross-sections of HMPs revealing a microsphere organization of the particles (Fig. 8). Furthermore, it can be noticed that the freeze-dried microspheres were well-isolated and formed powders with good rheological behaviors.

Size measurements put in evidence that for all of HMPs, volume size distributions (Fig. 5) followed an almost Gaussian curve around 50-60 µm with reasonable spans between 1.38 and 1.67 (Table 3). A slight asymmetry towards high values of size was also observed. We supposed that it was due to a coalescence phenomenon between the emulsification step and the thermogel freeze during the TSE process. D[4,3] ranged from 54.9 to 58 µm and were quite close to the VMD. In contrast, D[3,2] were much lower (from 19.9 to 22.6 µm) highlighting the presence of a significant number of small particles (Piacentini, 2014). A Kruskal-Wallis test on summarized results in Table 3 proved that there is no statistically significant difference between all HMPs, neither in D[4,3] nor D[3,2]. We concluded that particle sizes were homogeneous and independent from the physicochemical properties of the ICO engaged, underlining the predominance of the mechanical stirring influence.

The hybrid structure of HMPs was the result of the vegetable oil cross-linking by means of mineral bonds, during a sol-gel reaction. At the molecular scale, this chemical reaction proceeds in two phases: a first one of ethoxysilanes hydrolysis leads to free silanols which, during the second phase of condensation, can react between them to form siloxanes bonds (Si-O-Si). To offset the progressive inactivation of the catalyst SnOct in the TSE aqueous medium (oxidation of Sn II into Sn IV), the use of a co-catalyst was investigated to accelerate

HMP synthesis down to one week rather than one month. It was previously reported that the ethoxysilanes residue hydrolysis increases using acetic acid in a co-catalysis mechanism firstly described by Andrianov (Andrianov, 1965). An anionic substitution of the acetyl- moieties leads to an ethyl-acetate further eliminated during the microparticle recovery (Pope and Mackenzie, 1986). To confirm the influence of the acetic medium on the efficiency of cross-linking, infrared spectra were recorded on HMPs formulated in deionized water (HMPw) or in acetic buffer (HMPa) using ICO as reference (Fig. 6).

The absorbances at 952, 1075 and 1102 cm^{-1} were assigned to the ethoxysilanes (Si-O-CH_2-CH_3) (Leyden and Atwater, 1991; Silverstein et al., 2005, p. 124). An enhanced hydrolysis of the ethoxysilanes moieties was observed for HMPa related to HMPw. In addition, the broad-band around 1000 cm^{-1} attributed to overlapping of the −Si−O−Si− and −C−Si−O− stretching peaks (Allauddin et al., 2013) underscores the efficiency of the condensation in HMPa spectrum. To ensure that the acidic pH did not alter the triglyceride structure, especially the ester bond between glycerol and ricinoleate, microdroplets of CO formulated in the same conditions were analyzed by ^{1}H NMR spectroscopy and the result showed that the ester bond remained stable despite the low pH (data not shown). In addition and according to the literature (Shafiei et al., 2017), the ethyl-acetate generated during ICO formulation does not trans-esterify the ricinolein in mild conditions.

CP-MAS experiments in ^{29}Si-NMR spectroscopy enhanced the response of silicon nuclei and perfectly identified the chemical shifts of non condensed (T^0), partially (T^1, T^2) and fully condensed (T^3) silica species (Fig. 1) in the hybrid network at -48, -53, -57 and -67 ppm, respectively. The different natures of silica bonds between the ICOs monomers were quantified by complementary SP-MAS experiments as summarized in Table 4 and Fig.A.2.

Unexpectedly, SP-MAS spectra presented a sharp peak (from 0.2 to 0.6 ppm wide) at -45 ppm with decreasing values from 39.9 % for HMP 1.05 to 1.7 % for HMP 0.6. As far as we searched in literature, we did not find any description on such thin peak during solid-state ^{29}Si NMR experiment in SP-MAS conditions. We supposed that it was a liquid-state profile with averaged anisotropic interactions and a liquid-state ^{29}Si NMR experiment was consequently conducted on uncross-linked ICO 1.05 (Fig. A.3). A strong peak was detected at -45.7 ppm and assigned to liquid-state ICO monomers of which none of the silanol functions had reacted (liquid peak = LP) whereas the T^0 peak represent non-condensed silica species in solid-state

(i.e. connected to the hybrid network by other silica species present on the same ICO monomer). To quantify the sol-gel cross-linking, condensation yields (CY in eq. 3) were calculated:

$$\mathbf{CY} = \mathbf{100}\% - \mathbf{LP} \qquad \textbf{(3)}$$

A correcting factor (1/CY) was then used to calculate accurate condensation degrees (CD in eq. 4):

$$\mathbf{CD} = \frac{\mathbf{T^1 + 2T^2 + 3T^3}}{\mathbf{3 \times CY}} \qquad \textbf{(4)}$$

Owing to the variable intensity of the liquid peak, CDs evolved from 60.1 to 98.3 % for HMP 1.05 and HMP 0.6, respectively, meaning that high silylation ratios did not permit an efficient condensation. It would seem that the sol-gel reaction had not occurred in some domains within high silylated HMPs. The rough surface of HMP 1.05 (Fig. 4-A) could be thus explained, on the assumption that particles partially "collapse" above liquid domains. Nevertheless, CDs which represent the ability of silylated precursors to bind to each other, were not complete (around 70-80 %) and similar for the three HMPs (1.05, 0.8 and 0.6). Indeed it was documented that alkylsilanes with long organic tails don't reach a complete condensation owing to an increase of steric hindrance (Delattre and Babonneau, 1994; Peeters et al., 1995). Moreover, multifunctional silica precursors are often limited to form single siloxane bonds (Brochier Salon and Belgacem, 2011).

TGA analyses were conducted in order to check the hybrid structure of HMPs (Fig. 7). For all samples, the weight-loss began approximately at 160 °C corresponding to the ibuprofen degradation (Lerdkanchanaporn and Dollimore, 1997). Then the dissociation of the urethane bond around 250 °C underscored the degradation onset of the hybrid matrix (Saunders, 1959). From 300 to 600 °C corresponding to the triglyceride disruption, the four curves differed: higher was the organic part, faster was the weight-loss (HMPs 0.4 > 0.6 > 0.8 > 1.05). Finally, a stabilization of the weights occurred after 650 °C, highlighting the mineral residue of each HMP. As expected, the values ranged from 7.4 to 14 % for the highest silylated sample (HMP 1.05) related to the lowest one (HMP 0.4).

It is well known that the location of the API in microspheres governs release kinetics from the matrices. Therefore, EDX analyses were performed on flurbiprofen-loaded HMPs to study the

API location inside the particles using its own fluorine atom as probe. 8 wt% flurbiprofen-loaded HMP 0.4 were cryofreezed prior to a mechanical shock. Firstly, EDX spectra of fluorine (K-L_2 and K-L_3 transition[§]), carbon (K-L_2 and K-L_3 transition) and silicium (K-L_3 transition) atoms were recorded on three HMP 0.4 cross-sections as illustrated in Fig. 8 and summarized in Table 5. Several positions in the inner and outer regions of HMP were recorded and similar values ranging from 0.37 to 0.52 % were measured attesting an almost homogeneous API distribution in the HMPs.

The same conclusion was deduced from the silicium and carbon atoms on the homogenous composition of the hybrid matrix even if the carbon was slightly overestimated due to undetermined hydrogen atoms. To support this observation, retro-scattered electrons from carbon and silicium were recorded on HMP 1.05 during 20 min producing an atomic map depicted in Fig. 9. Despite the presence of carbon in background and some electronic shadows due to the eccentric position of the SD Detector (at the top-right of the pictures), the scans exhibited a uniform disposition of carbon (Fig. 9– C) and silicium (Fig. 9– D) on particle surfaces. It should also be noted that less than 0.3 % of catalyst's tin was detected. In contrast with the TGA results on HMP 0.4 (i.e. 7.4 % of mineral residue), a smaller part of silicium (1.8 % in average of silicium, corresponding to 4 % in weight) was observed during EDX analyses on the same sample. The formation of silicon oxides throughout the thermal analysis under airflow was the cause of this overestimation.

3.3. Pharmaceutical characterization of hybrid microparticles

The drug delivery potential of HMPs was firstly explored measuring the encapsulation yield of ibuprofen in the particles. Two parameters varied in the formulations: the silylation ratio of the ICO (from 0.4 to 1.05) and the loading rate of ibuprofen (from 4 to 16 wt%). The silylation ratio was first tuned from 0.4 to 1.05 while the ibuprofen loading rate was set at 4 wt%. Ranging from 90 to 100 %, the encapsulation yields showed an almost complete encapsulation of the API with a slight downward trend with the decreased silylation ratio (Fig. 10). In fact, some ethoxysilanes might remained within highly silylated HMPs and the previous assumption (i.e. complete hydrolysis of ethoxysilanes) was not yet accurate in this case. Therefore, the **η'** (and consequently the encapsulation yields) might be overestimated. Second, the loading rate

[§] K-L_2 and K-L_3 refer to the electronic transitions between atomic orbitals after the X-ray excitation.

of ibuprofen was tuned from 4 to 16 wt% while the silylation ratio of the ICO was set at 1.05. The results exhibited also very satisfying yields up to 16 wt% loaded-HMP and no trend to loss of the API was noticed.

The crystallinity of the API is a key parameter that modulates the drug dissolution. Indeed crystalline drugs are thermodynamically more stable than amorphous ones and are thus less able to dissolve *in vivo* (Hancock and Parks, 2000). XRD spectra were recorded on pure ibuprofen and ibuprofen-loaded HMPs at various loading rates (Fig. 11). 4 and 8 wt% loaded-HMPs had an amorphous organization (large halo) highlighting a molecular solubilization of the ibuprofen within the particles. By contrast, 12 and 16 wt% loaded-HMPs exhibited specific peaks of crystallized ibuprofen at 6, 16.5, 17.5, 20, 22 and 25° of 2theta underlining the formation of API microcrystals inside these HMPs.

The XRD results were corroborated by supplementary DSC experiments (Fig. 11). The endothermic peak of the ibuprofen melting (around 76 °C) was detected for 12 and 16 wt% loaded-particles whereas 4 and 8 wt% ibuprofen-loaded HMPs presented no peak of melting meaning the molecular solubilization of ibuprofen within the latter matrices.

The release kinetics of ibuprofen from the particles were widely investigated. In order to respect sink conditions, all the media used ensured more than tenfold of ibuprofen solubility (Finholt and Solvang, 1968; Avdeef, 2007). Therefore ibuprofen release kinetics from HMPs depended only on the particle properties. To investigate the oral route, the release properties of 4 wt% ibuprofen-loaded HMPs 1.05 were studied in simulated digestive medium added by a surfactant (protocol **1 –** see Methods). The results depicted in Fig.A.4 showed a double stage release of the API. Ibuprofen being a carboxylic acid, it was protoned in acidic medium (SGF, pH= 1.2) whereas it lost its proton in neutral medium (SIF, pH= 6.8) accelerating its release from the matrix. The entire payload was then released after 3 hours.

A comprehensive study was done on the second stage of release (i.e. in SIF) using HMPs 0.4 to 1.05 loaded at 4 wt% of ibuprofen in order to highlight the influence of the silylation ratio (Fig. 12).

The results exhibited a definite trend in the release kinetics: the lower is the ratio, the faster is the release. The sizes of HMPs being statistically similar, the differences observed in release kinetics could only be explained by a difference in HMPs properties and their abilities to retain

the API. In case of LBDDS, the discussion remains open about the two models of “medium diffusion into the matrix” or the “API diffusion out of the matrix” as limiting, and thus controlling factors of release (Siepmann and Siepmann, 2011). However, the use of a biorelevant medium to mimic the physiological conditions especially in term of pH and surface tension overcomes these considerations as it ensures an optimal *in vitro / in vivo* correlation. In other hand, Xu (Xu et al., 2009) demonstrated that the change in surface state of mesoporous silica nanoparticles by grafting trimethylsilane (an hydrophobic agent) was sufficient to slowdown the release of API without changing the matrix composition, the wettability of the particles is consequently a significant factor. The potential impact of the HMPs surface states was annihilated in our study by optimizing the wettability of the HMPs and by setting the amount of the wetting agent at 0.1 wt% for all experiments. In order to quantify the differences in internal structure of the matrices, the release kinetics were mathematically simulated from which the diffusion coefficients (D) of ibuprofen were deduced. Taking into consideration EDX, XRD and DSC results (i.e. homogeneity of the API within the spheres and its molecular state), 4 wt% ibuprofen-loaded HMPs were related to monolithic solutions in which a molecular dissolution of the API happened (Siepmann and Siepmann, 2012). Therefore, an appropriate release model was implemented (Appendix B). The fitting optimization was carried out by least squares method (Fig. 13) and the diffusion coefficient (D) of ibuprofen in each HMP was then deducted (Table 6).

The diffusion coefficients of ibuprofen ranged from 1.44 $.10^{-9}$ to 7.28 $.10^{-9}$ $cm^2.s^{-1}$ according to the HMP type. They increased by a seven factor when the X_R decreased from 1.05 to 0.4. Considering ^{29}Si NMR results, the condensation yields seemed to follow the same trend whereas the condensation degrees were similar. It suggests that the release from effectively cross-linked matrices is facilitated and the liquid fraction within ICO 1.05 and 0.8 exhibited a solubilization capacity towards ibuprofen and thus slowed down its release. These diffusion coefficients in our matrices are in same range with ones reported on classical materials such as the diffusion of ibuprofen in a mesoporous magnesium carbonate material “Upsalite®” (9.8 $.10^{-8}$ $cm^2.s^{-1}$) (Zhang et al., 2016) which permitted an extended-release on 24 h in phosphate buffer. Similarly, ibuprofen diffusion coefficients were determined in polyester-based microparticles and were found to be 4.18 $.10^{-12}$ and 6.59 $.10^{-10}$ $cm^2.s^{-1}$, for PLLA and PLGA

respectively (Lee et al., 2012); ibuprofen release in these systems occurred over 70 days (in phosphate buffer).

Finally to consider the subcutaneous route as a potential administration route, release kinetics of 4 wt% ibuprofen-loaded HMPs 1.05 were recorded in PBS medium (Fig. 14). A first stage of "burst" effect was noted where 35 % (3.39 µmol) of the API was released in 50 h. However, a second stage of sustained release exhibited a slope of 5 % per 50 hours (9.7 nmol per hour). It can be explained by the poor dispersibility and wettability of the HMPs in PBS buffer that makes full sense to the hypothesis of water diffusion control (Siepmann and Siepmann, 2011). Indeed in absence of surfactant, HMPs tend to form a cluster that favors a sustained release by the slow diffusion of the API from the core to the surface of the insert-like material.

3.4. Biological characterization of hybrid microparticles:

As noted above, HMPs presented an interesting potential for oral and subcutaneous drug delivery. Therefore, the digestibility and the cytotoxicity of these particles were studied. Fig. 15 shows the pH drop of digestion media containing CO or the HMPs. The fitted curve of CO digestion was used as reference and it exhibited a linear decrease of pH during the 1.5 h of the experiment highlighting a constant degradation rate of the ester bonds. However, HMPs curves demonstrated an exponential decrease of pHs with an initial drop higher than the one of CO curve, followed by a slowing after 45 min of digestion. We supposed that the hydrolysis of the particles was limited to the surface due to the inability of lipase to catalyze the rupture of deeper ester bonds. Indeed silylated Fatty Acids (FA)s are linked to the matrix by two kinds of bonds: the ester and the siloxane. The ester bond could be hydrolyzed by the lipase while the siloxane remains stable preventing the catalytic progression of the enzyme. This hypothesis is in line with the more significant pH decrease recorded for HMP 0.4 compared to others, because of their high content of non-silylated FA.

In order to support this hypothesis, HMPs 1.05 loaded with 1 wt% of Sudan Black B (SBB) were synthesized and subjected to the same digestion protocol. The SBB allowed us to track the black HMPs within the digestion medium. After 2 h of digestion, the dye diffused in the medium but the morphology of HMP seemed to be preserved confirming the surface-limited digestion of the particles (Fig. 16).

The cytotoxity studies of the four HMPs at different concentrations were conducted on two kinds of cells simulating the digestive (Caco-2) and the subcutaneous (NIH-3T3 fibroblasts) cellular environments. Briefly, satisfying results were reached and the elements extracted from HMPs had not induced cell death in both cases (Fig. 17). For Caco-2/TC7 enterocytes, the cell viability varied from 80 to 120 % without a trend dependent on microparticle concentration or X_R and this cellular type seems little sensitive. On the contrary, two trends were observable for the fibroblasts assays: the influence of the HMP concentration and their X_R. The cell viability decreased from 100 to 70 % by increasing the concentration from 0.1 to 10 $mg \cdot mL^{-1}$ or by decreasing the silylation ratio from 1.05 to 0.4. An explanation to this slight viability decrease could be related to the release of FFA from 0.4 HMP leading to the acidification of the culture medium. Concerning the influence of the concentration that was already observed (Gallon et al., 2017), we could attribute it to the presence of carrageenan residues. However, viability results were higher than 84 % below this excessive concentration of 10 $mg \cdot mL^{-1}$. Thus we could consider that HMPs are well tolerated.

4. Conclusion

An original approach to formulate poorly water-soluble APIs in vegetable oil / silica hybrid microparticles (HMPs) was described. A complete oil silylation in solvent- and catalyst-free conditions was reached whatever the oil / silica ratio used, and the TSE process was optimized for pharmaceutical application exhibiting a good robustness with high preparation yields (> 85 %) in all formulations. This process produced solid and microspheric particles in which the API was homogeneously disposed. For ibuprofen, excellent encapsulation yields were reached up to 16 wt% of ibuprofen-loaded HMPs. Futhermore, two behaviors of the loaded-API were highlighted: an amorphous solubilization up to 8 wt% then a microcrystalline dispersion up to 16 wt% of ibuprofen. A tunability of API release from HMPs was underscored and depended on two physicochemical parameters. First, the wettability of the HMPs, which is connected to the biorelevant medium used, induced a complete API release ranging from 3 hours (in simulated intestinal fluid) up to 15 days (in subcutaneous simulated medium). Second, the structure of the HMP matrix, which depends on the silylation ratio of the CO and the sol-gel condensation yield and degree, led to a slowdown of API release when the uncross-linked amount of ICO increased. These releases were also mathematically fitted to the diffusion model from a sphere described by Crank and the diffusion coefficients D were then deducted.

Finally, a surface-limited digestion of the HMPs by means of lipases was highlighted and a good cytocompatibility was exhibited on fibroblasts and enterocyte-like cells.

5. Appendix A: Supporting Data

Fig. A.1. Chemical structures of ibuprofen and flurbiprofen (from European Pharmacopeia 9.5)

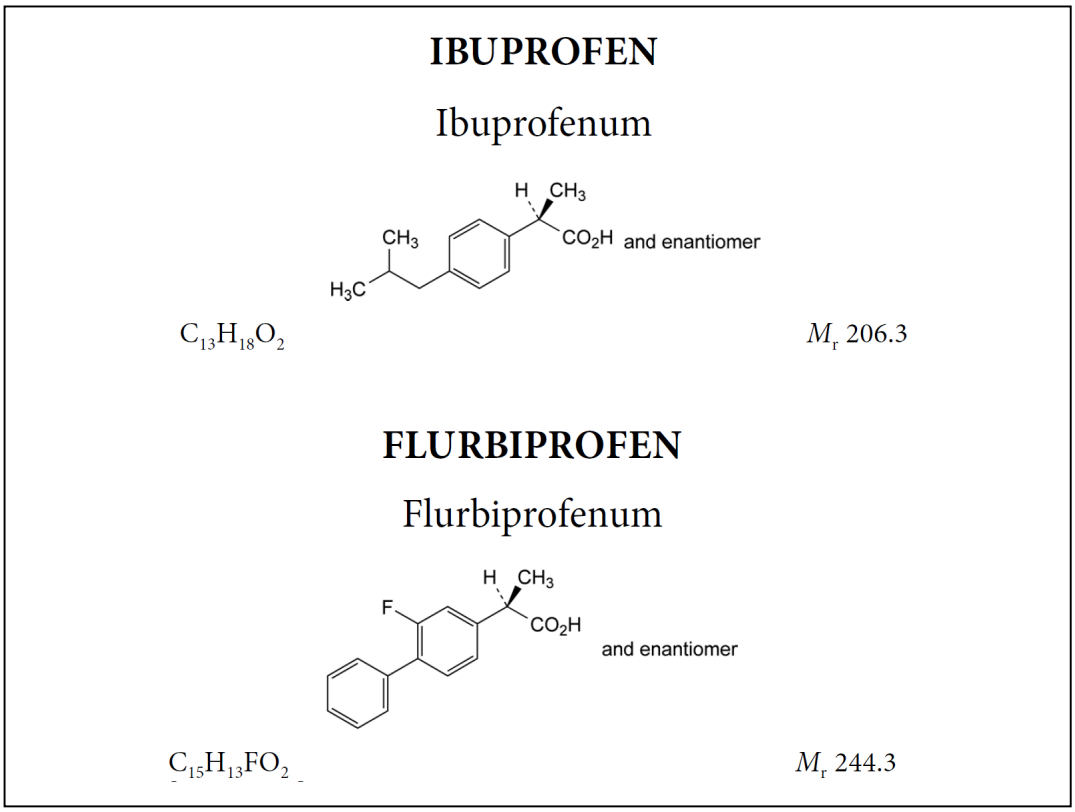

Fig. A.2. ^{29}Si NMR spectra of HMPs: a) 1.05 b) 0.8 c) 0.6 . Spectra were fitted and area under curves for SP-MAS experiments were integrated in percent.

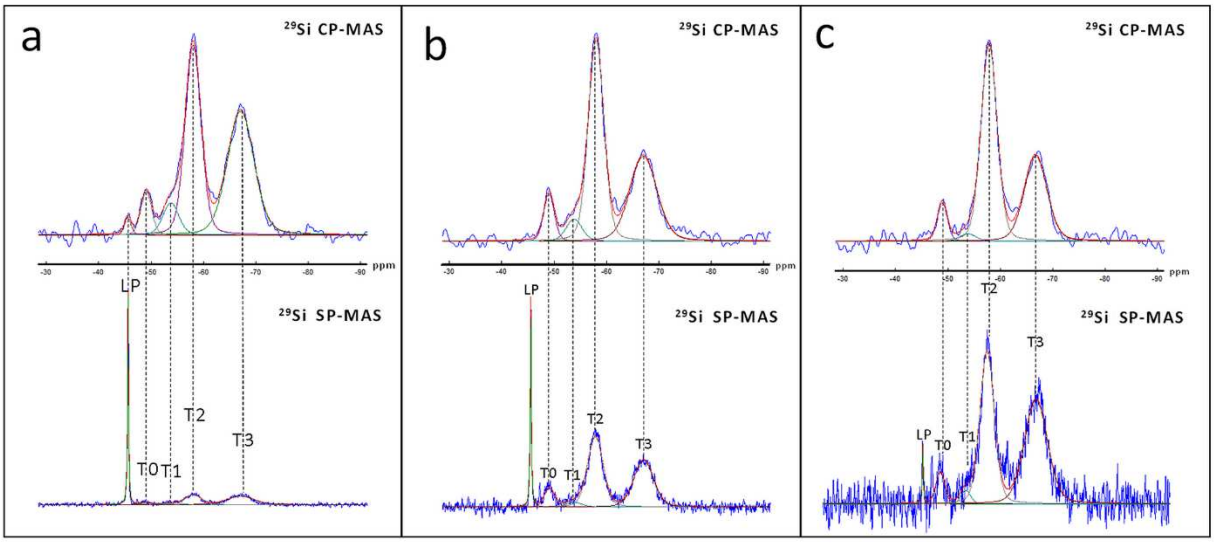

Fig. A.3. ^{29}Si NMR of ICO 1.05. The peak at -46.6 ppm was assigned to the excess of IPTES, and the one at -45.4 ppm to an impurity initially present in the reagent.

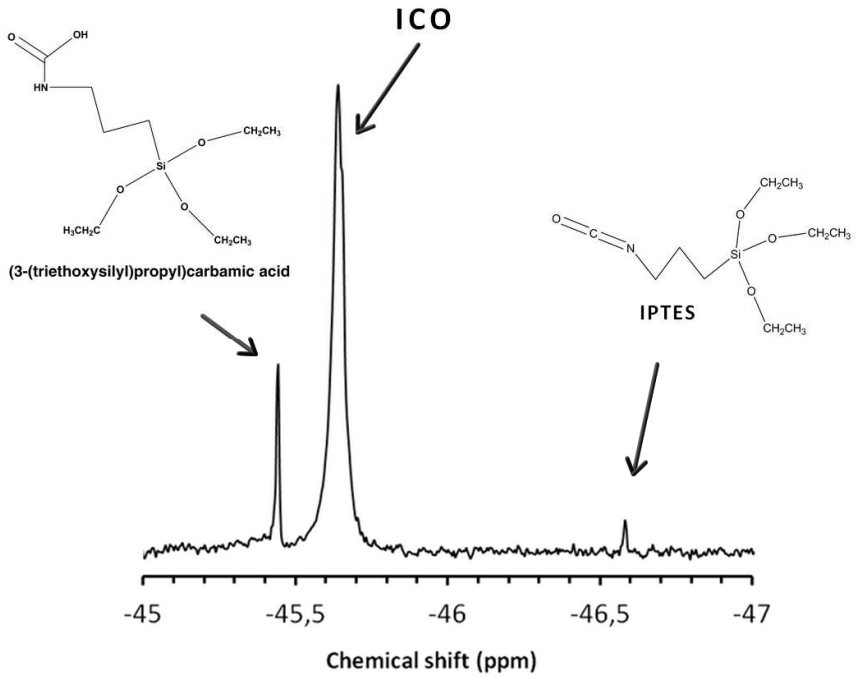

Fig. A.4. Release kinetics from 4 wt% ibuprofen-loaded HMPs 1.05 in Simulated Gastric and Intestinal Fluids (SGF and SIF respectively). n=3.

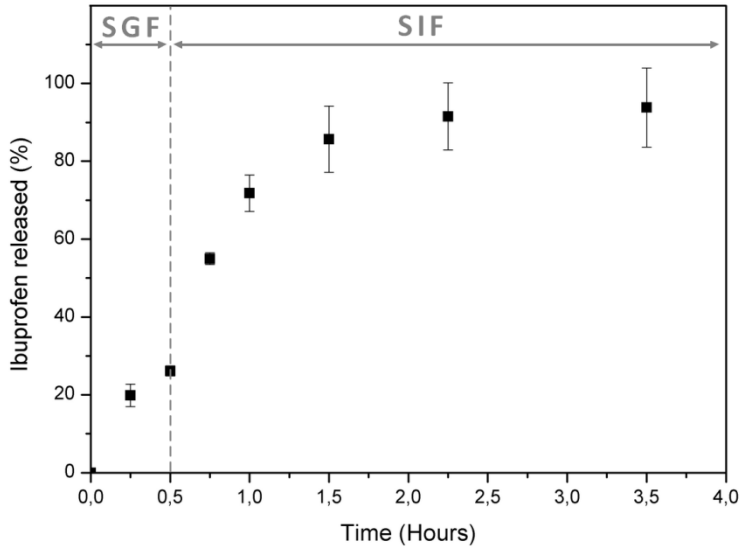

537

538 **Table A.1. Composition of the HMPs digestion medium for biodegradability assays**

		Component	Concentration	Purpose
Digestion medium	Pre-digestion medium	PBS buffer	6 mM of phosphate	Buffering the medium at pH = 6.8
		Porcine bile extract	5 mM	Emulsifying the substract
		Phospholipids (S 100 Lipoïd)	1.25 mM	
		Pancreatin (4 × USP)	450 UA	Hydrolysis of glycerol-fatty acid bonds
		Ca^{2+}	36mM aqueous solution 1mL injected every 15mn	Precipitation of free fatty acids (FFA)s

539

6. Appendix B: Mathematical Modeling

Considering that:

- An optimal wettability has been ensured on HMPs;
- The API is homogeneously and amorphously disposed within HMPs;
- The HMPs are not significantly swelling or eroding during API release (surface-limited digestion).
- Sink conditions are provided in the release media.

A mathematical model for 4 wt% ibuprofen-loaded HMPs releases in Simulated Intestinal Fluid (SIF) was established referring to the diffusion equation in spheres (Crank, 1975, p. 91):

$$M(R,t) = M_\infty(R) - M_\infty(R)\frac{6}{\pi^2}\sum_{n=1}^{N\to\infty}\frac{\exp\left(-\frac{Dn^2\pi^2 t}{R^2}\right)}{n^2} \quad \text{(B.1)}$$

Where $M(t)$ and M_∞ are the cumulative amounts of ibuprofen released at time "t" and at infinite time, respectively. D is the diffusion coefficient of the ibuprofen within the particle, and R is the radius of this particle.

The cumulative amounts of ibuprofen at infinite time depends on three parameters, C_1, C_0 and R, which represent the concentration at the surface of the sphere, the initial concentration within the sphere and the radius of the particle, respectively (Zhang, 2008, p. 226).

$$M_\infty(R) = (C_0 - C_1) \times V = (C_0 - C_1)\frac{4\pi R^3}{3} \quad \text{(B.2)}$$

It is important to note that $M(t)$ and M_∞ are both R dependent. As the amount of released ibuprofen is additive, then the total of released ibuprofen depends on the size distribution of HMPs at a given radius ($P(R)$):

$$M(t) = \overline{M(R,t)} = \int_{R_{min}}^{R_{max}} M(R,t)\, P(R)\, \mathrm{d}R \quad \text{(B.3)}$$

$$\overline{M(R,t)} = \overline{M_\infty(R)} - \overline{M_\infty(R)\frac{6}{\pi^2}\sum_{n=1}^{N\to\infty}\frac{\exp\left(-\frac{Dn^2\pi^2 t}{R^2}\right)}{n^2}} \quad \text{(B.4)}$$

559

$$\frac{\overline{M(R,t)}}{\overline{M_\infty(R)}} = 1 - \frac{1}{\overline{M_\infty(R)}}\overline{M_\infty(R)\frac{6}{\pi^2}\sum_{n=1}^{N\to\infty}\frac{\exp\left(-\frac{Dn^2\pi^2 t}{R^2}\right)}{n^2}} \quad \text{(B.5)}$$

560

$$\frac{\overline{M(R,t)}}{\overline{M_\infty(R)}} = 1 - \frac{1}{\overline{R^3}}\overline{R^3\frac{6}{\pi^2}\sum_{n=1}^{N\to\infty}\frac{\exp\left(-\frac{Dn^2\pi^2 t}{R^2}\right)}{n^2}} \quad \text{(B.6)}$$

561 The size distribution of HMPs (*N(R)*) can be obtained experimentally by Laser diffraction
562 particle sizing technique, and used to calculate the $\overline{R^3}$ and $\overline{R^3\frac{6}{\pi^2}\sum_{n=1}^{N\to\infty}\frac{\exp\left(-\frac{Dn^2\pi^2 t}{R^2}\right)}{n^2}}$:

$$\overline{R^3} = \int_{R_{min}}^{R_{max}} R^3\, P(R)\, \mathrm{d}R \quad \text{(B.7)}$$

563

$$\overline{R^3\frac{6}{\pi^2}\sum_{n=1}^{N\to\infty}\frac{\exp\left(-\frac{Dn^2\pi^2 t}{R^2}\right)}{n^2}} = \int_{R_{min}}^{R_{max}} R^3\frac{6}{\pi^2}\sum_{n=1}^{N\to\infty}\frac{\exp\left(-\frac{Dn^2\pi^2 t}{R^2}\right)}{n^2}\, P(R)\, \mathrm{d}R \quad \text{(B.8)}$$

564

565 The eq. (B.6) was used to fit the experimental data points, using the non-linear least square
566 method, and the GNU Octave software (leasqr function). To work out the eq. (B.6), we used
567 the experimental size distribution of particles and the trapeze method to estimate integrals in

568 the eqs. (B.7) and (B.8). Finally, the solver was used in order to extract the diffusion coefficient
569 (D) of ibuprofen in each HMP.

ACKNOWLEDGEMENTS

Authors are willing to thank Laurent Mercier for his technical assistance, Emmanuel Fernandez, Aurélien Lebrun and Karine Parra for their technical assistance and advices in NMR, Didier Cot for Scanning Electronic Microscopy photographs and Caroline Laurent for kindly supplying the Caco-2 cells. Authors thank the Algerian government for the PhD grant and the Franco-Algerian steering committee for its support.

REFERENCES

Allauddin, S., Narayan, R., Raju, K.V.S.N., 2013. Synthesis and Properties of Alkoxysilane Castor Oil and Their Polyurethane/Urea–Silica Hybrid Coating Films. ACS Sustainable Chemistry & Engineering 1, 910–918. https://doi.org/10.1021/sc3001756

Andrianov, K.A., 1965. Metalorganic Polymers, Interscience. ed, Polymer Reviews. John Wiley & Sons Inc, New York.

Avdeef, A., 2007. Solubility of sparingly-soluble ionizable drugs. Advanced Drug Delivery Reviews 59, 568–590. https://doi.org/10.1016/j.addr.2007.05.008

Brinker, C.J., 1988. Hydrolysis and condensation of silicates: Effects on structure. Journal of Non-Crystalline Solids 100, 31–50. https://doi.org/10.1016/0022-3093(88)90005-1

Brochier Salon, M.-C., Belgacem, M.N., 2011. Hydrolysis-Condensation Kinetics of Different Silane Coupling Agents. Phosphorus, Sulfur, and Silicon and the Related Elements 186, 240–254. https://doi.org/10.1080/10426507.2010.494644

Cannon, C.G., 1976. Infrared frequencies of amide, urea, and urethane groups. The Journal of Physical Chemistry 80, 1247–1248. https://doi.org/10.1021/j100552a026

Chen, D., Yazdi, S., 2013. Polymer- and Lipid-Based Systems for Parenteral Drug Delivery, in: Kolhe, P., Shah, M., Rathore, N. (Eds.), Sterile Product Development. Springer New York, New York, NY, pp. 47–60. https://doi.org/10.1007/978-1-4614-7978-9_3

Crank, J., 1975. The mathematics of diffusion, 2d ed. ed. Clarendon Press, Oxford, [Eng].

Delattre, L., Babonneau, F., 1994. Influence of the nature of the R Group on the Hydrolysis and Condensation Process of Trifunctional Silicon Alkoxides, R-Si(OR')3. MRS Proceedings 346. https://doi.org/10.1557/PROC-346-365

Department of Health and Human Services, 2018. CFR - Code of Federal Regulations (No. 21), Food and Drugs. FOOD AND DRUG ADMINISTRATION.

Efentakis, M., Dressman, J.B., 1998. Gastric juice as a dissolution medium: surface tension and pH. Eur J Drug Metab Pharmacokinet 23, 97–102.

Finholt, P., Solvang, S., 1968. Dissolution kinetics of drugs in human gastric juice--the role of surface tension. J Pharm Sci 57, 1322–1326.

Gallon, G., Lapinte, V., Robin, J.-J., Chopineau, J., Devoisselle, J.-M., Aubert-Pouëssel, A., 2017. Cross-Linked Castor Oil-Based Hybrid Microparticles as Drug Delivery Systems. ACS Sustainable Chemistry & Engineering 5, 4311–4319. https://doi.org/10.1021/acssuschemeng.7b00369

Hancock, B.C., Parks, M., 2000. What is the true solubility advantage for amorphous pharmaceuticals? Pharm. Res. 17, 397–404. https://doi.org/10.1023/A:1007516718048

Kalepu, S., Manthina, M., Padavala, V., 2013. Oral lipid-based drug delivery systems – an overview. Acta Pharmaceutica Sinica B 3, 361–372. https://doi.org/10.1016/j.apsb.2013.10.001

Klein, S., 2010. The Use of Biorelevant Dissolution Media to Forecast the In Vivo Performance of a Drug. The AAPS Journal 12, 397–406. https://doi.org/10.1208/s12248-010-9203-3

Kruse, C.G., Timmerman, H., Solvay Pharmaceuticals (Eds.), 2008. Towards drugs of the future: key issues in lead finding and lead optimization, Solvay Pharmaceuticals Conferences. IOS Press, Amsterdam ; Washington, D.C.

Lee, W.L., Shi, W.-X., Low, Z.Y., Li, S., Loo, S.C.J., 2012. Modeling of drug release from biodegradable triple-layered microparticles: Modeling of Drug Release. Journal of Biomedical Materials Research Part A 100A, 3353–3362. https://doi.org/10.1002/jbm.a.34292

Lerdkanchanaporn, S., Dollimore, D., 1997. A thermal analysis study of Ibuprofen. Journal of thermal analysis 49, 879–886. https://doi.org/10.1007/BF01996773

Leyden, D.E., Atwater, J.B., 1991. Hydrolysis and condensation of alkoxysilanes investigated by internal reflection FTIR spectroscopy. Journal of Adhesion Science and Technology 5, 815–829. https://doi.org/10.1163/156856191X00233

Li, Y., Li, J., Ma, S., Luo, Y., 2016. Different catalytic systems on hydroxyl-terminated GAP and PET with poly-isocyanate: Curing kinetics study using dynamic *in situ* IR spectroscopy. International Journal of Polymer Analysis and Characterization 21, 495–503. https://doi.org/10.1080/1023666X.2016.1175202

Low, S.P., Voelcker, N.H., Canham, L.T., Williams, K.A., 2009. The biocompatibility of porous silicon in tissues of the eye. Biomaterials 30, 2873–2880. https://doi.org/10.1016/j.biomaterials.2009.02.008

Mangione, M.R., Giacomazza, D., Bulone, D., Martorana, V., Cavallaro, G., San Biagio, P.L., 2005. K+ and Na+ effects on the gelation properties of κ-Carrageenan. Biophysical Chemistry 113, 129–135. https://doi.org/10.1016/j.bpc.2004.08.005

Massiot, D., Fayon, F., Capron, M., King, I., Le Calvé, S., Alonso, B., Durand, J.-O., Bujoli, B., Gan, Z., Hoatson, G., 2002. Modelling one- and two-dimensional solid-state NMR spectra: Modelling 1D and 2D solid-state NMR spectra. Magnetic Resonance in Chemistry 40, 70–76. https://doi.org/10.1002/mrc.984

Mosgaard, M.D., Sassene, P., Mu, H., Rades, T., Müllertz, A., 2015. Development of a high-throughput in vitro intestinal lipolysis model for rapid screening of lipid-based drug delivery systems. European Journal of Pharmaceutics and Biopharmaceutics 94, 493–500. https://doi.org/10.1016/j.ejpb.2015.06.028

Niemeyer, C., Mirkin, C.A., 2007. Nanobiotechnology II: more concepts and applications. Wiley-VCH, Weinheim.

Paprskářová, A., Možná, P., Oga, E.F., Elhissi, A., Alhnan, M.A., 2016. Instrumentation of Flow-Through USP IV Dissolution Apparatus to Assess Poorly Soluble Basic Drug Products: a Technical Note. AAPS PharmSciTech 17, 1261–1266. https://doi.org/10.1208/s12249-015-0444-4

Peeters, M.P.J., Wakelkamp, W.J.J., Kentgens, A.P.M., 1995. A 29Si solid-state magic angle spinning nuclear magnetic resonance study of TEOS-based hybrid materials. Journal of Non-Crystalline Solids 189, 77–89. https://doi.org/10.1016/0022-3093(95)00248-0

Piacentini, E., 2014. Droplet Size, in: Drioli, E., Giorno, L. (Eds.), Encyclopedia of Membranes. Springer Berlin Heidelberg, Berlin, Heidelberg, pp. 1–2. https://doi.org/10.1007/978-3-642-40872-4_1690-1

Pope, E.J.A., Mackenzie, J.D., 1986. Sol-gel processing of silica: II. The role of the catalyst. Journal of Non-Crystalline Solids 87, 185–198. https://doi.org/10.1016/S0022-3093(86)80078-3

Pouton, C.W., Porter, C.J.H., 2008. Formulation of lipid-based delivery systems for oral administration: Materials, methods and strategies. Advanced Drug Delivery Reviews 60, 625–637. https://doi.org/10.1016/j.addr.2007.10.010

Rawle, A., 2018. Basic principles of particle size analysis.

Saunders, J.H., 1959. The Reactions of Isocyanates and Isocyanate Derivatives at Elevated Temperatures. Rubber Chemistry and Technology 32, 337–345. https://doi.org/10.5254/1.3542399

Shafiei, A., Rastegari, H., Ghaziaskar, H.S., Yalpani, M., 2017. Glycerol transesterification with ethyl acetate to synthesize acetins using ethyl acetate as reactant and entrainer. Biofuel Research Journal 4, 565–570. https://doi.org/10.18331/BRJ2017.4.1.7

Shi, X., Graiver, D., Narayan, R., 2012. Hydrolysis and Condensation of Hydrophilic Alkoxysilanes Under Acidic Conditions. Silicon 4, 109–119. https://doi.org/10.1007/s12633-012-9108-0

Siepmann, J., Siepmann, F., 2012. Modeling of diffusion controlled drug delivery. J Control Release 161, 351–362. https://doi.org/10.1016/j.jconrel.2011.10.006

Siepmann, J., Siepmann, F., 2011. Mathematical modeling of drug release from lipid dosage forms. International Journal of Pharmaceutics 418, 42–53. https://doi.org/10.1016/j.ijpharm.2011.07.015

Siewert, M., Dressman, J., Brown, C.K., Shah, V.P., FIP, AAPS, 2003. FIP/AAPS guidelines to dissolution/in vitro release testing of novel/special dosage forms. AAPS PharmSciTech 4, E7. https://doi.org/10.1208/pt040107

Silverstein, R.M., Webster, F.X., Kiemle, D., 2005. Spectrometric Identification of Organic Compounds, 7th Edition. Wiley.

Socrates, G., 2010. Infrared and Raman characteristic group frequencies: tables and charts, 3. ed., as paperback. ed. Wiley, Chichester.

Stippler, E., Kopp, S., Dressman, J.B., 2004. Comparison of US Pharmacopeia Simulated Intestinal Fluid TS (without pancreatin) and Phosphate Standard Buffer pH 6.8, TS of the International Pharmacopoeia with Respect to Their Use in In Vitro Dissolution Testing. Dissolution Technologies 11, 6–10. https://doi.org/10.14227/DT110204P6

Wissing, S.A., Kayser, O., Müller, R.H., 2004. Solid lipid nanoparticles for parenteral drug delivery. Adv. Drug Deliv. Rev. 56, 1257–1272. https://doi.org/10.1016/j.addr.2003.12.002

Xu, W., Gao, Q., Xu, Y., Wu, D., Sun, Y., Shen, W., Deng, F., 2009. Controllable release of ibuprofen from size-adjustable and surface hydrophobic mesoporous silica spheres. Powder Technology 191, 13–20. https://doi.org/10.1016/j.powtec.2008.09.001

Xu, W., Riikonen, J., Lehto, V.-P., 2013. Mesoporous systems for poorly soluble drugs. International Journal of Pharmaceutics 453, 181–197. https://doi.org/10.1016/j.ijpharm.2012.09.008

699 Zangenberg, N.H., Müllertz, A., Kristensen, H.G., Hovgaard, L., 2001. A dynamic in vitro
700 lipolysis model. I. Controlling the rate of lipolysis by continuous addition of calcium.
701 Eur J Pharm Sci 14, 115–122.

702 Zhang, P., Zardán Gómez de la Torre, T., Forsgren, J., Bergström, C.A.S., Strømme, M., 2016.
703 Diffusion-Controlled Drug Release From the Mesoporous Magnesium Carbonate
704 Upsalite ®. Journal of Pharmaceutical Sciences 105, 657–663.
705 https://doi.org/10.1002/jps.24553

706 Zhang, Y., 2008. Geochemical kinetics. Princeton University Press, Princeton, N.J.

707

Fig.1. At the top: the silylation process of castor oil by means of IPTES, the ICO 1.05 (fully silylated) is represented. At the bottom: chemical structure of silica species in various condensation states.

Fig. 2. Formulation of the HMPs by an optimized Thermo-Stabilized oil-in-water Emulsion (TSE) process. The blue dots and the purple dashes describe the evolution of the system temperature and the viscosity of the water phase, respectively.

Fig. 3. FTIR monitoring of the castor oil silylation at various X_R. Red: ICO 1.05; Brown: ICO 0.8; Blue: ICO 0.6; Purple: ICO 0.4.

Fig.4. Scanning electronic microscopy observations of: a) HMPs 1.05 b) HMPs 0.8 c) HMPs 0.6 d) HMPs 0.4.

Fig. 5. Volume size distributions of the HMPs with four X_R. Each curve displays mean of n=3.

Fig. 6. IR-ATR spectra of silylated castor oil (ICO) and hybrid microparticles formulated in acetic buffer (HMPa) or in dezionised water (HMPw). The Fig. attest to the enhancement of ethoxysilanes hydrolysis when the acetic buffer was used.

Fig.7. TGA curves and mineral residues of 4 wt% ibuprofen-loaded HMPs formulated with multiple ICOs (from 0.4 to 1.05).

Fig.8. EDX spectra (sp.) recorded on cross-section of 8 % flurbiprofen-loaded HMPs. Each measurement was done on a $1\mu m^3$ dot.

Fig.9. EDX analysis of HMP 1.05: a) SEM image b) carbon / silicium map c) carbon map d) silicium map (the background is made from carbon).

Fig.10. On the left: encapsulation yields of HMPs for various silylation ratios, loaded with 4 % of ibuprofen. On the right: encapsulation yields of HMP 1.05 loaded with various rates of ibuprofen. n=3.

Fig. 11. X-ray powder diffractograms and differential scanning calorimetry of ibuprofen-loaded HMPs at: a) 4 % b) 8 % c) 12 % d) 16 % and of e) pure ibuprofen. The Y scale in the X-ray diffractogram “e” was increased three folds for more convenience.

Fig. 12.Release kinetics from 4 wt% ibuprofen -loaded HMPs in Simulated Intestinal Fluid (pH=6.8). n=3 and the minus error bars were hidden for more clarity.

Fig. 13. Experimental and mathematical modeling release kinetics of ibuprofen from HMPs. squares: experimental data; line: computed fits. Mt= ibuprofen released at time “t”; Minf= ibuprofen released at infinite time.

Fig. 14. Release kinetics of 4 wt% ibuprofen-loaded HMP 1.05 in PBS (pH=7.4). The experiment was stopped after 350 hours. n=3.

Fig. 15. pH drop versus time of digestion media containing ICO or HMPs. n=2

Fig.16. Sudan Black B-loaded HMP a) before and b) after 2 hours in a simulated digestion medium containing lipases.

Fig.17. Cytotoxicity studies of HMPs conducted on Caco-2/TC7 enterocytes and NIH-3T3 fibroblasts.

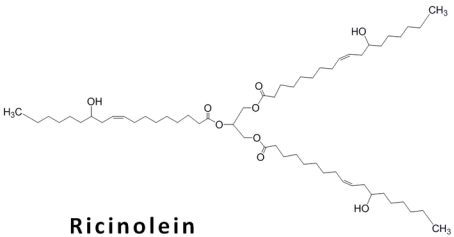

Ricinolein

60 °C , 72h

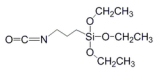

IPTES

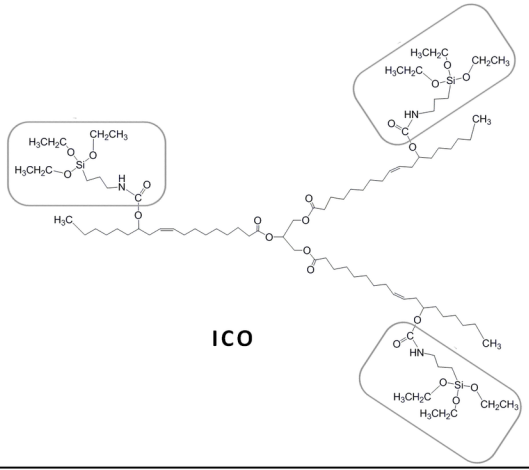

ICO

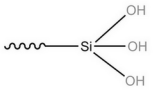

LP or T^0

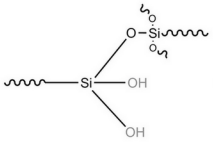

T^1

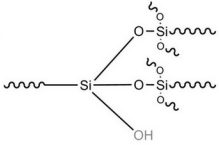

T^2

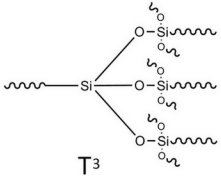

T^3

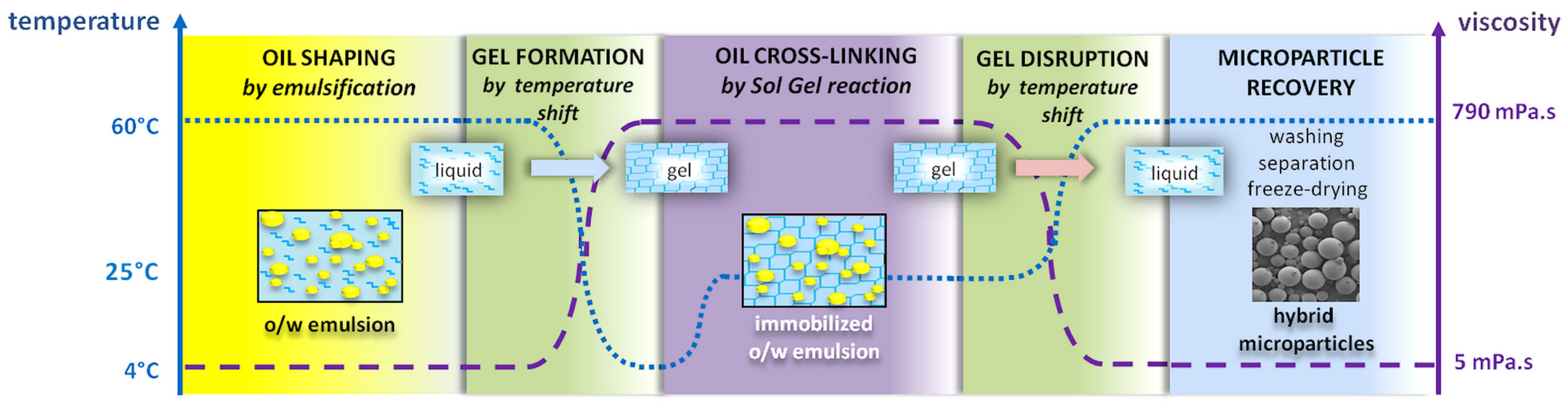
temperature
viscosity
OIL SHAPING
by emulsification
GEL FORMATION
by temperature shift
OIL CROSS-LINKING
by Sol Gel reaction
GEL DISRUPTION
by temperature shift
MICROPARTICLE RECOVERY
60°C
25°C
4°C
790 mPa.s
5 mPa.s
liquid
gel
gel
liquid
washing
separation
freeze-drying
o/w emulsion
immobilized
o/w emulsion
hybrid
microparticles

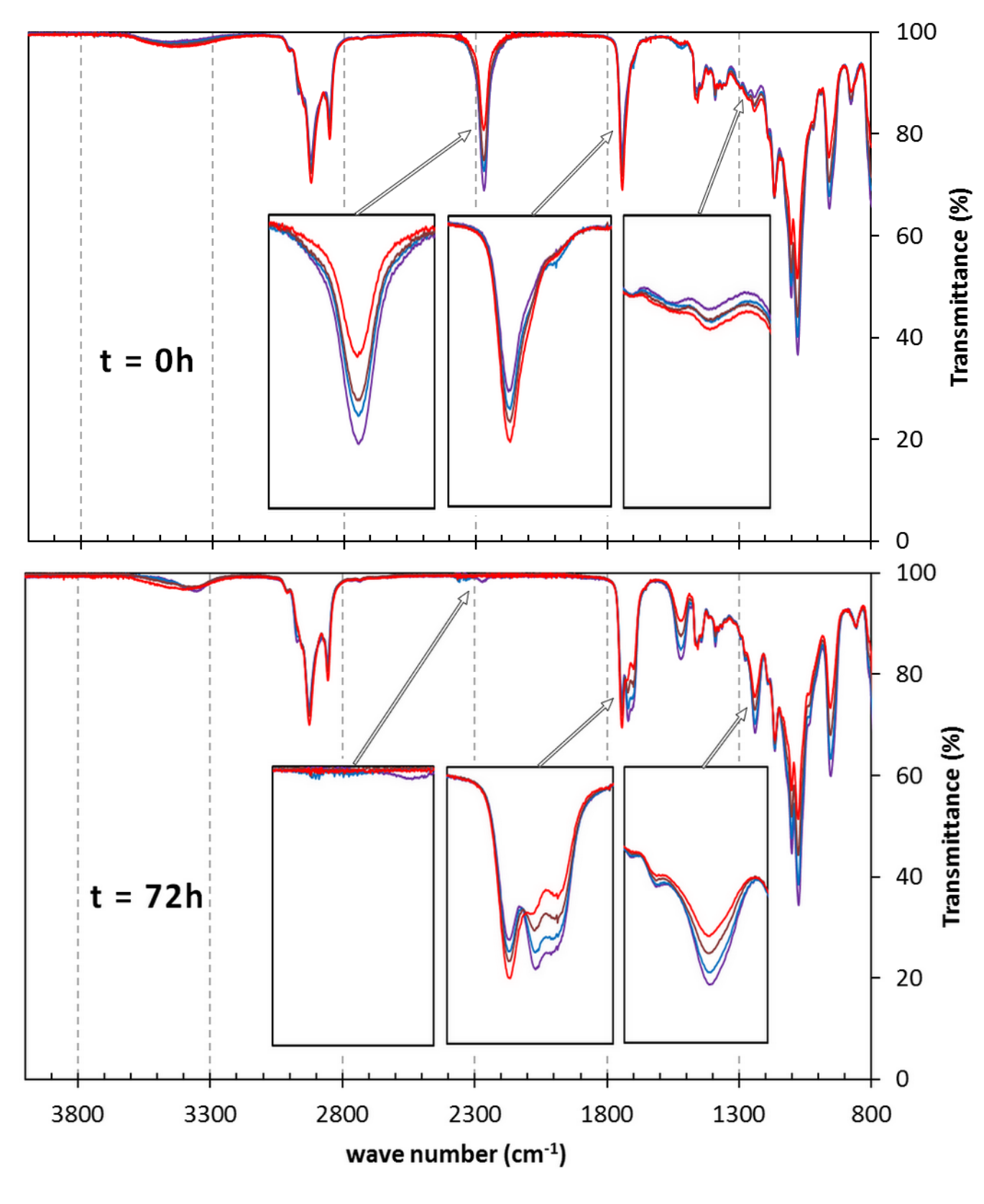
t = 0h
t = 72h
100
80
60
40
20
0
Transmittance (%)
3800
3300
2800
2300
1800
1300
800
wave number (cm-1)

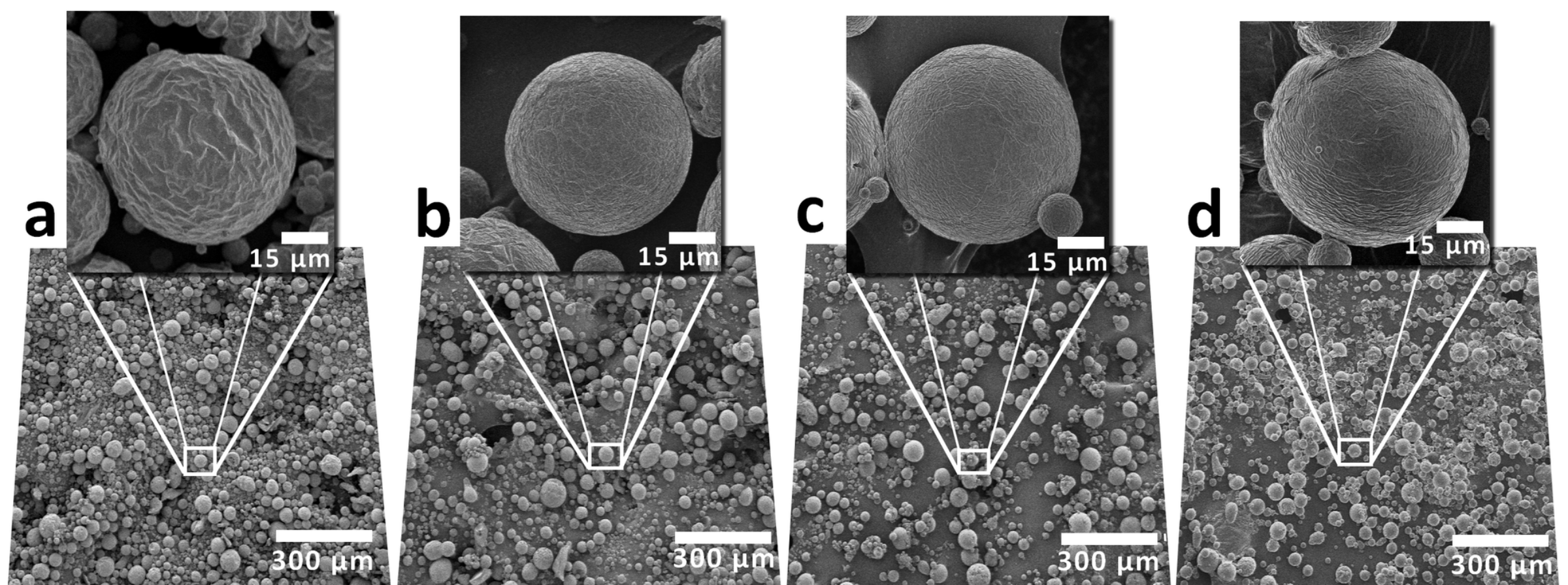
a
15 µm
300 µm
b
15 µm
300 µm
c
15 µm
300 µm
d
15 µm
300 µm

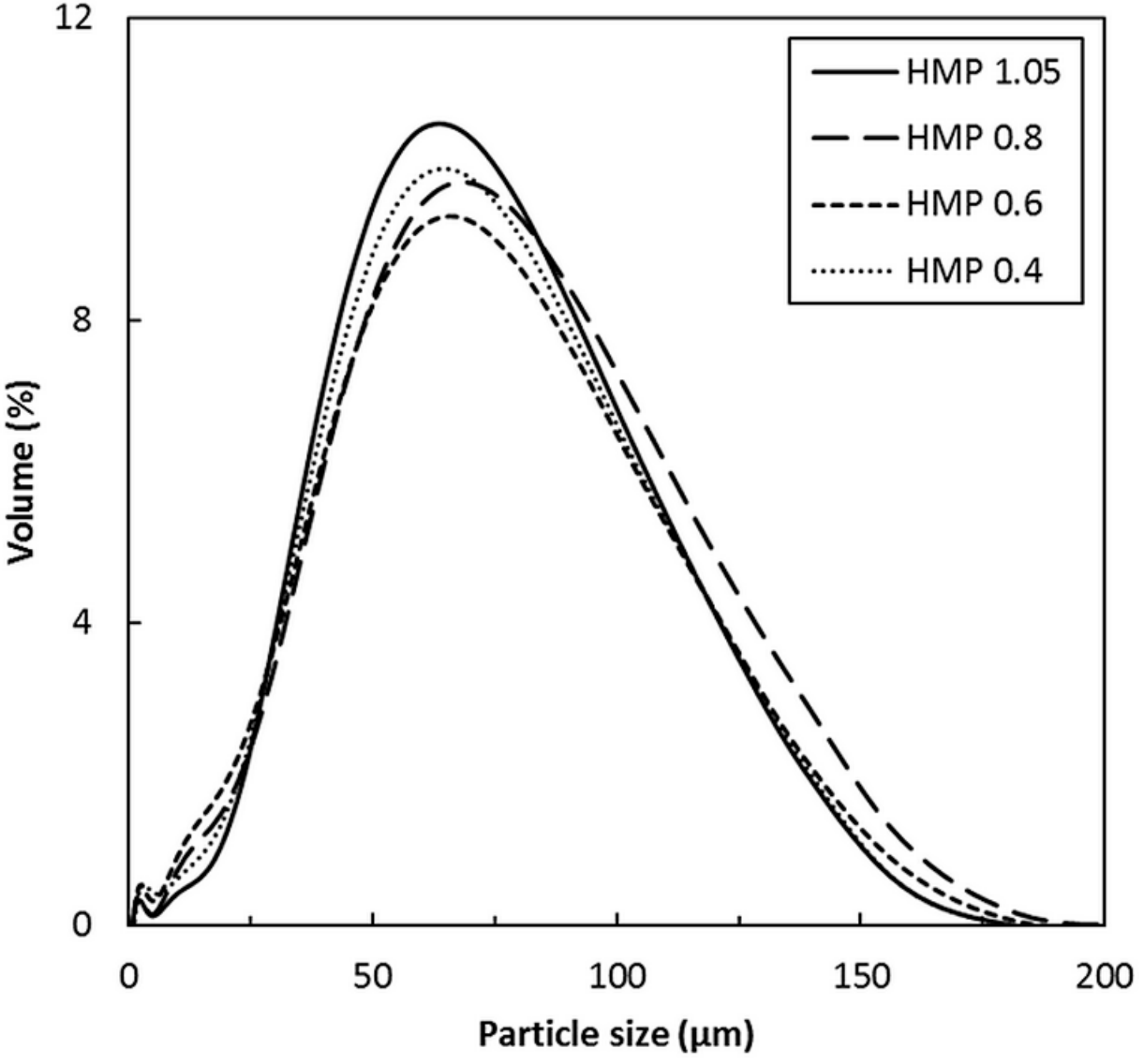
12
8
4
0
Volume (%)
0
50
100
150
200
Particle size (µm)
HMP 1.05
HMP 0.8
HMP 0.6
HMP 0.4

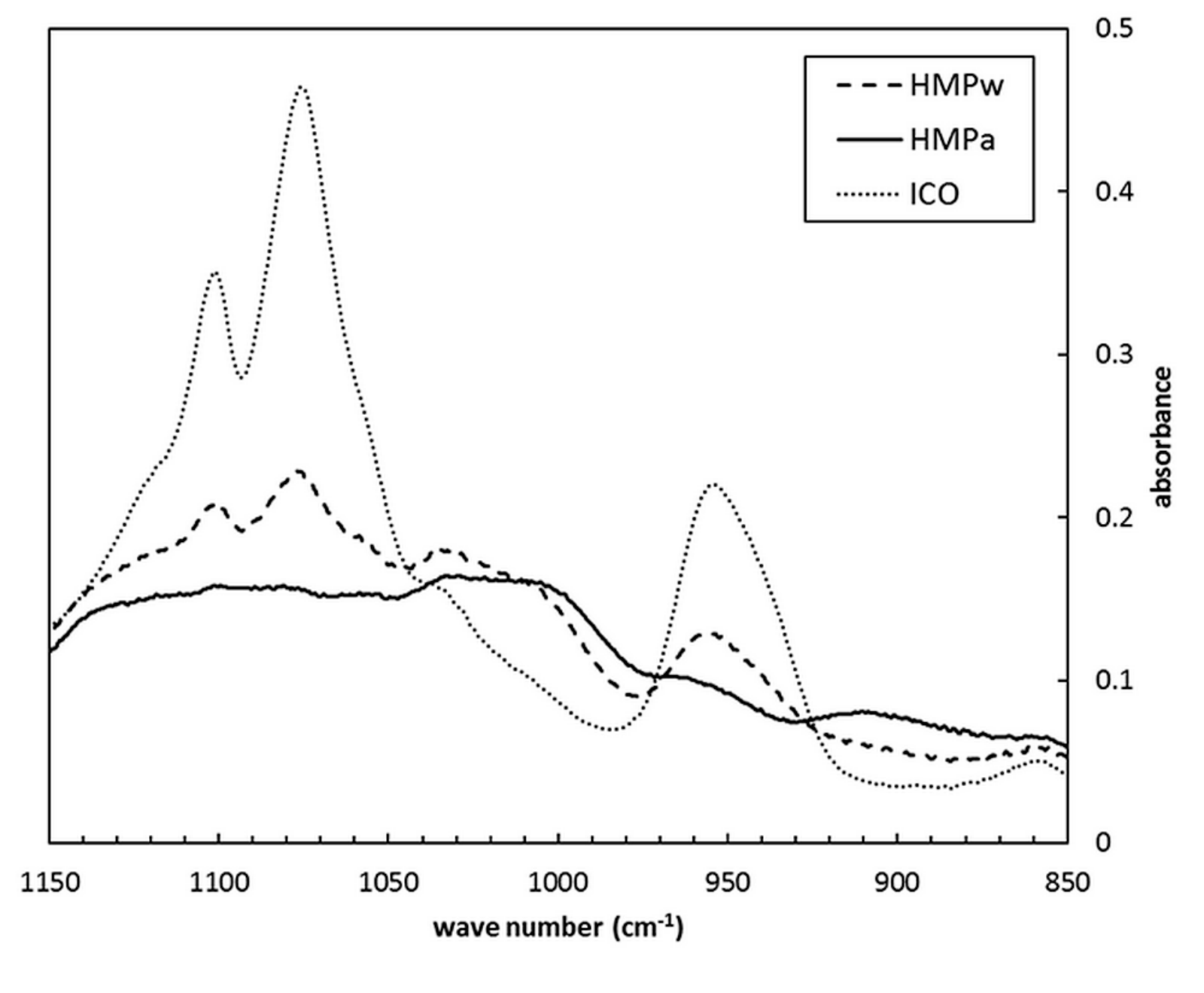
HMPw
HMPa
ICO
0.5
0.4
0.3
0.2
0.1
0
absorbance
1150
1100
1050
1000
950
900
850
wave number (cm-1)

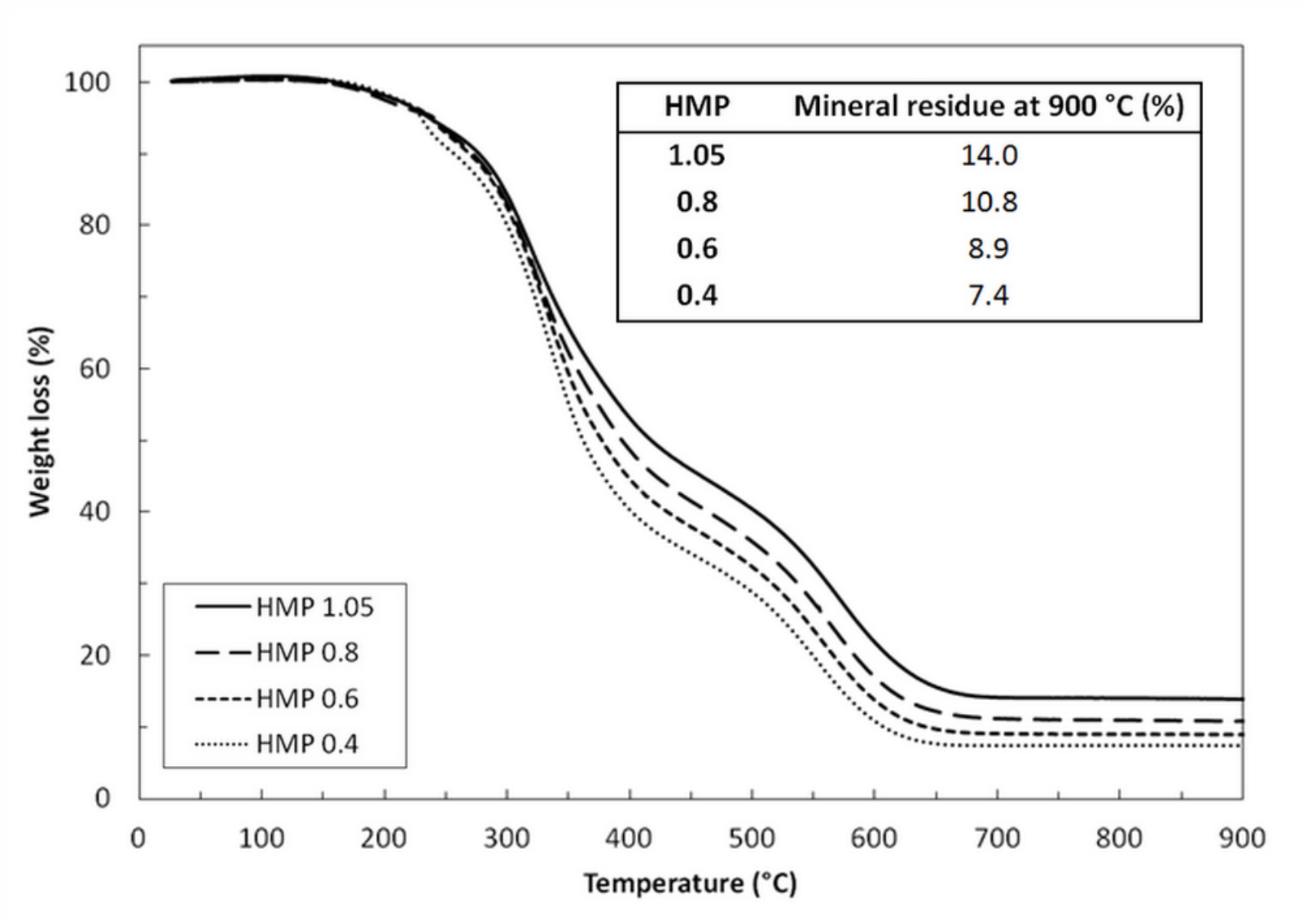
HMP | Mineral residue at 900 °C (%)
1.05 | 14.0
0.8 | 10.8
0.6 | 8.9
0.4 | 7.4
HMP 1.05
HMP 0.8
HMP 0.6
HMP 0.4
Weight loss (%)
Temperature (°C)
0
20
40
60
80
100
0
100
200
300
400
500
600
700
800
900

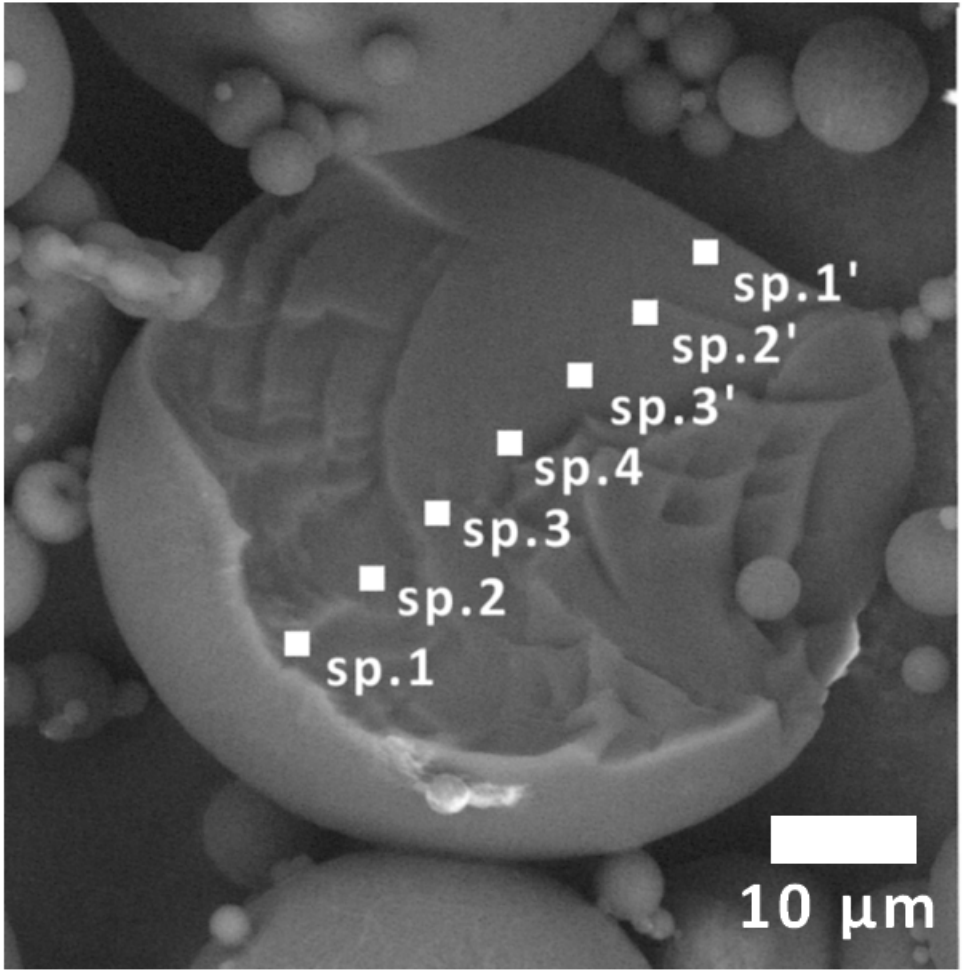
sp.1'
sp.2'
sp.3'
sp.4
sp.3
sp.2
sp.1
10 µm

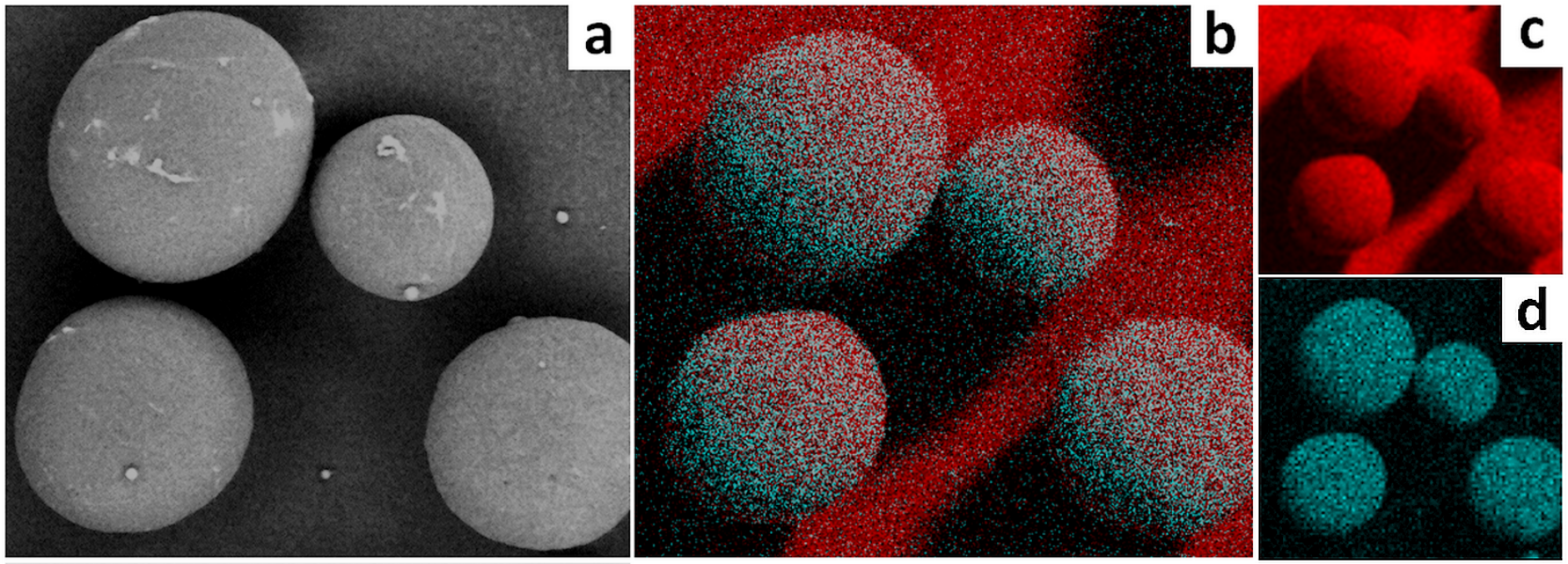
a
b
c
d

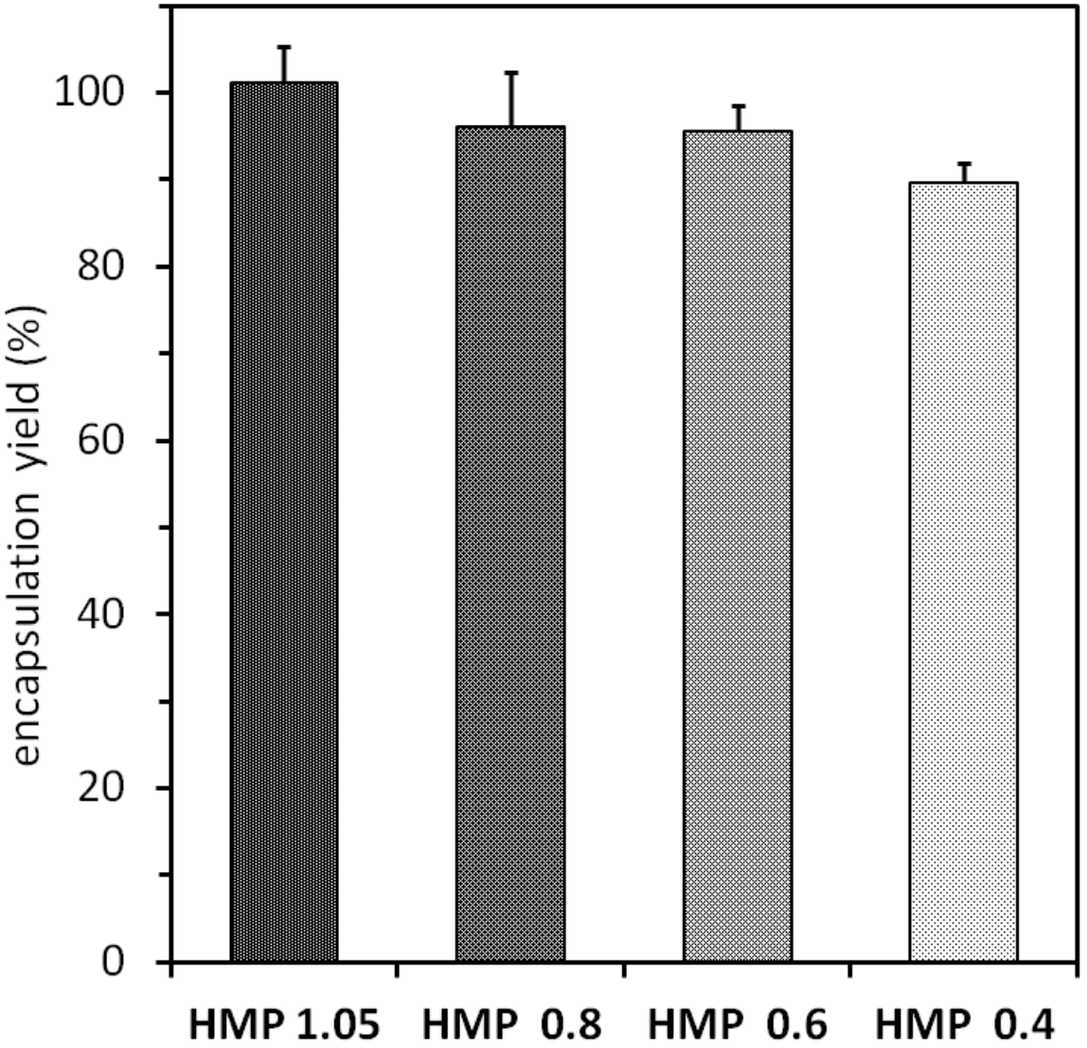
encapsulation yield (%)
100
80
60
40
20
0
HMP 1.05
HMP 0.8
HMP 0.6
HMP 0.4

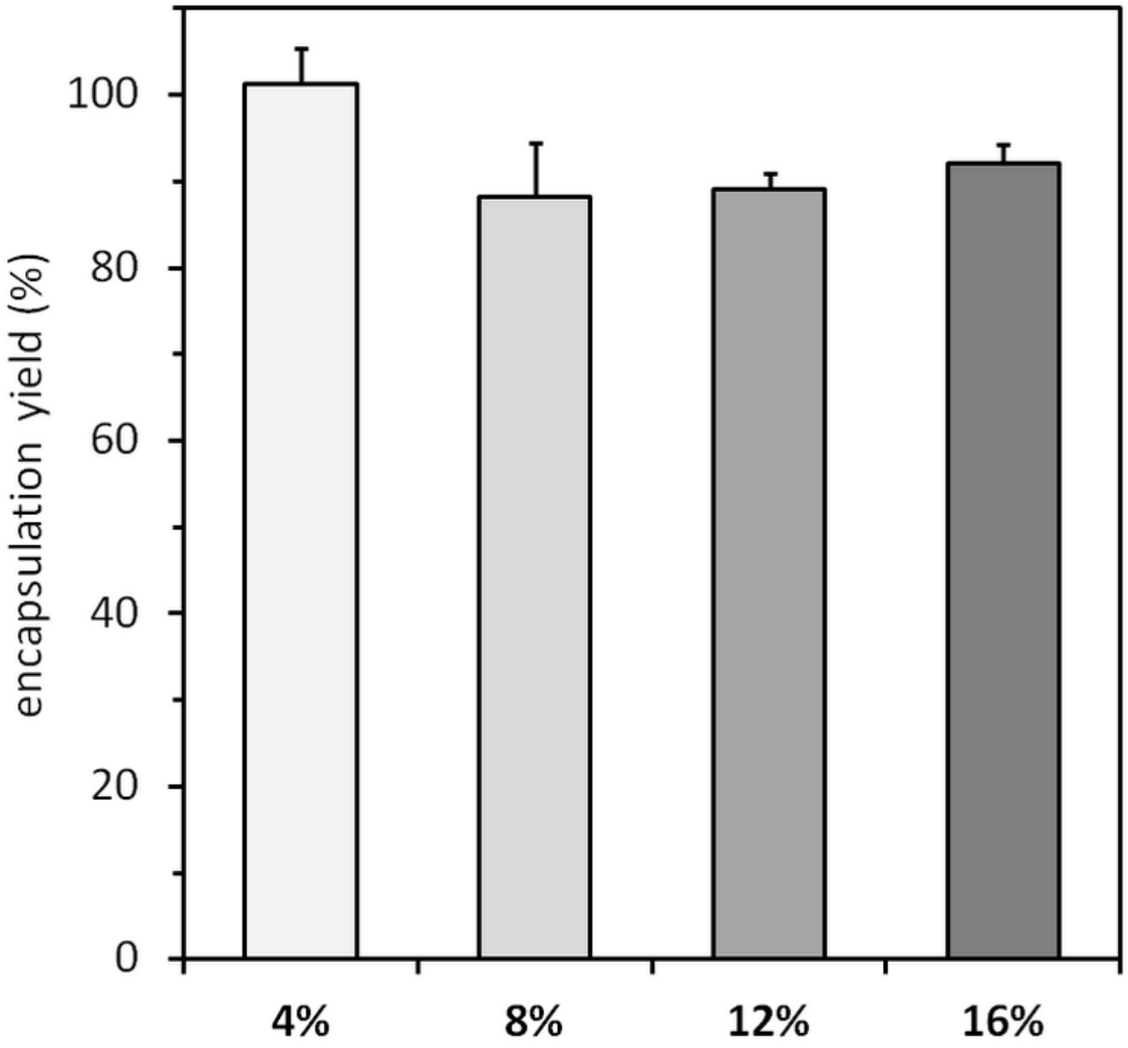
encapsulation yield (%)
100
80
60
40
20
0
4%
8%
12%
16%

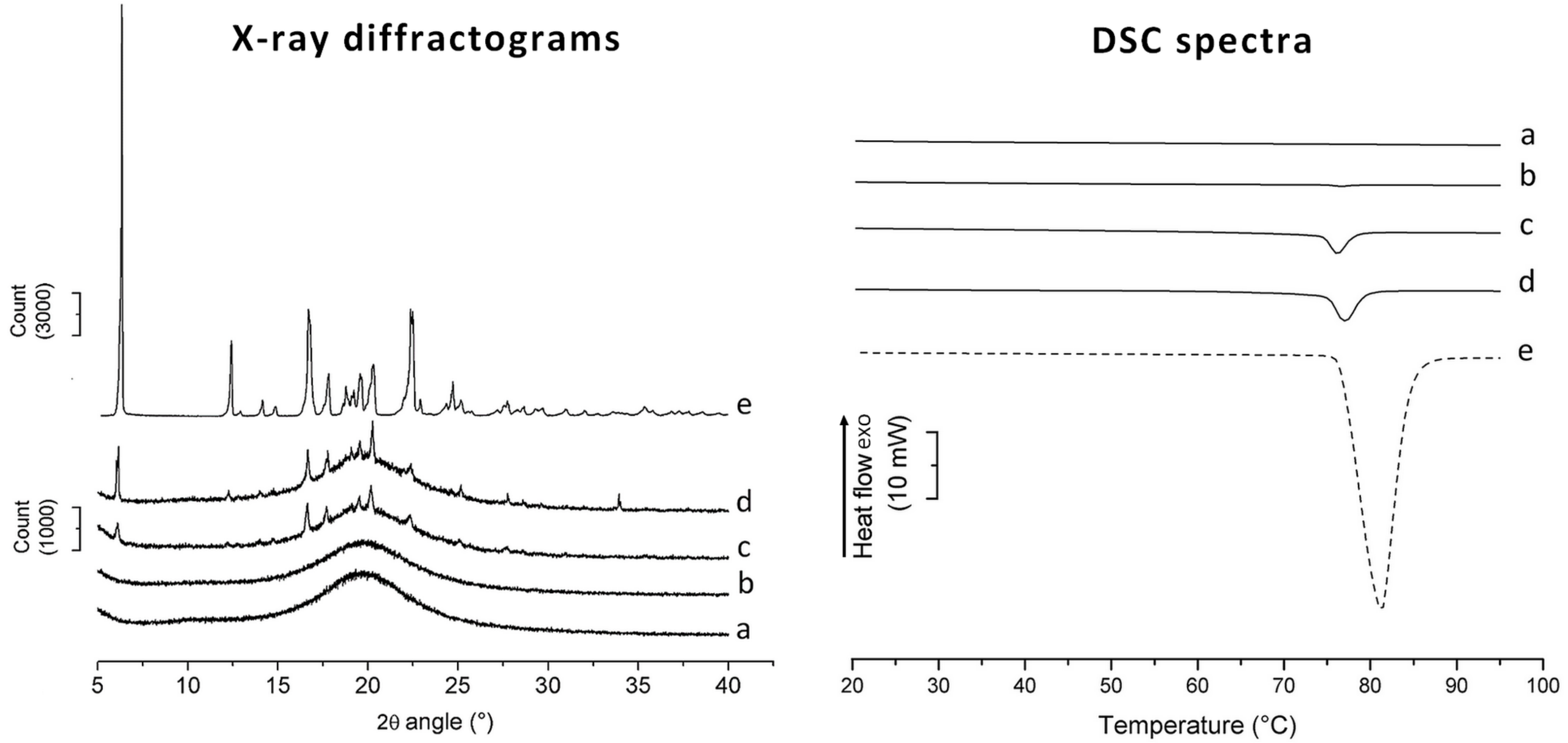
X-ray diffractograms
Count (3000)
Count (1000)
e
d
c
b
a
5
10
15
20
25
30
35
40
2θ angle (°)
DSC spectra
a
b
c
d
e
Heat flow exo
(10 mW)
20
30
40
50
60
70
80
90
100
Temperature (°C)

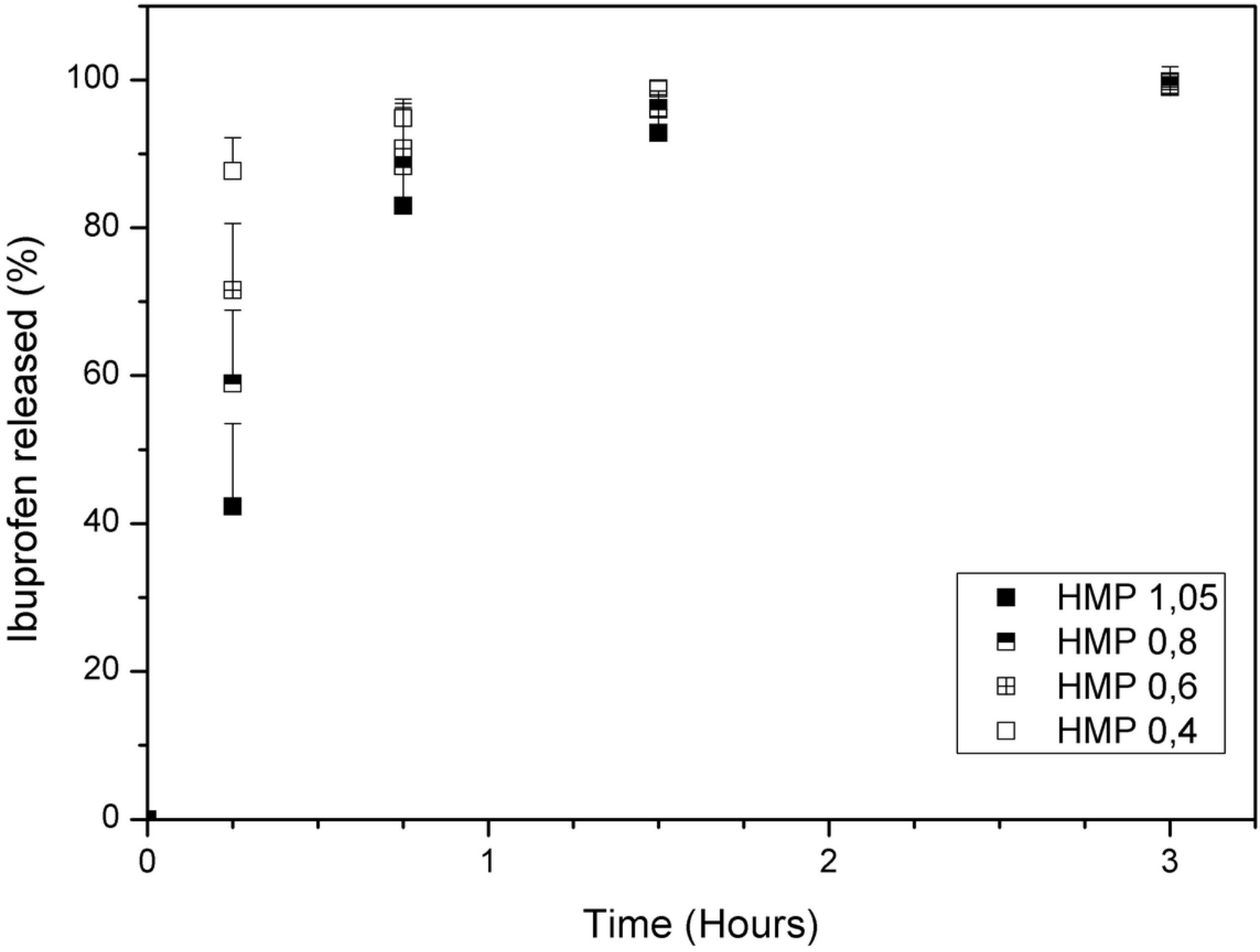
Ibuprofen released (%)
100
80
60
40
20
0
0
1
2
3
Time (Hours)
HMP 1,05
HMP 0,8
HMP 0,6
HMP 0,4

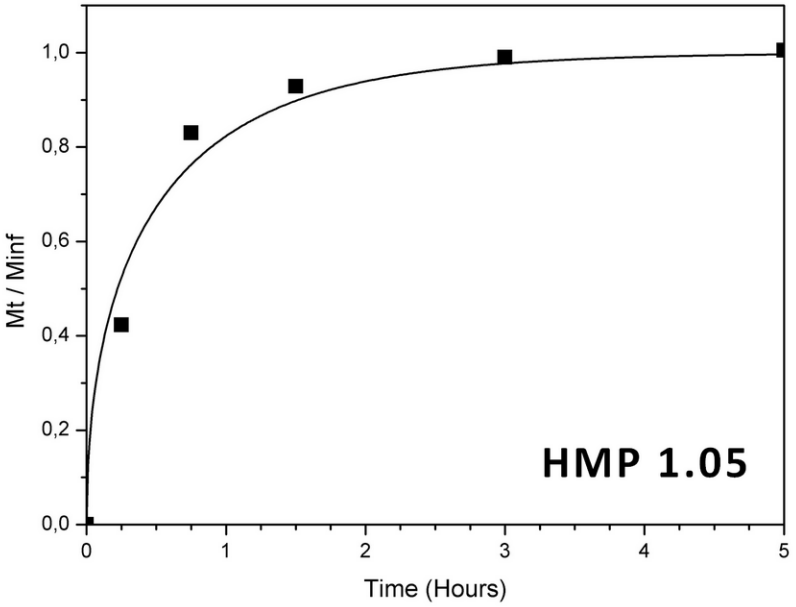
Mt / Minf
1,0
0,8
0,6
0,4
0,2
0,0
0
1
2
3
4
5
Time (Hours)
HMP 1.05

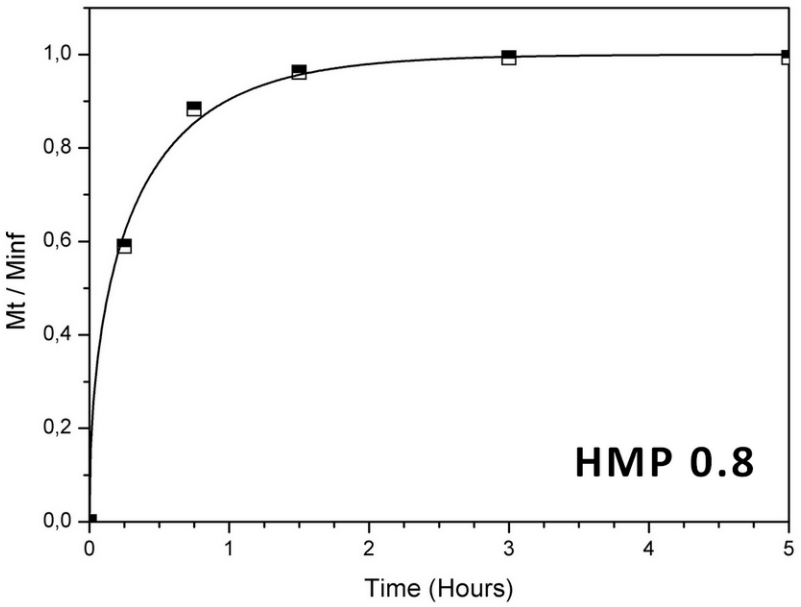
Mt / Minf
1,0
0,8
0,6
0,4
0,2
0,0
0
1
2
3
4
5
Time (Hours)
HMP 0.8

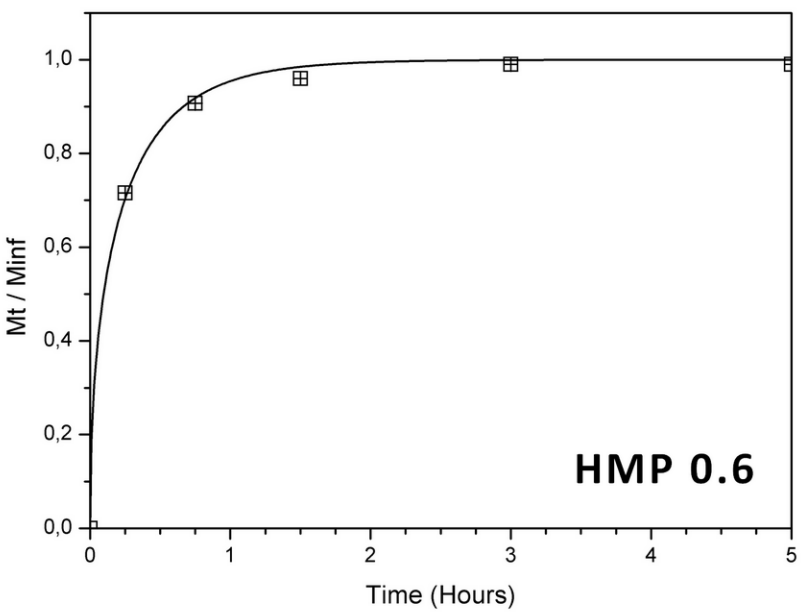
Mt / Minf
1,0
0,8
0,6
0,4
0,2
0,0
0
1
2
3
4
5
Time (Hours)
HMP 0.6

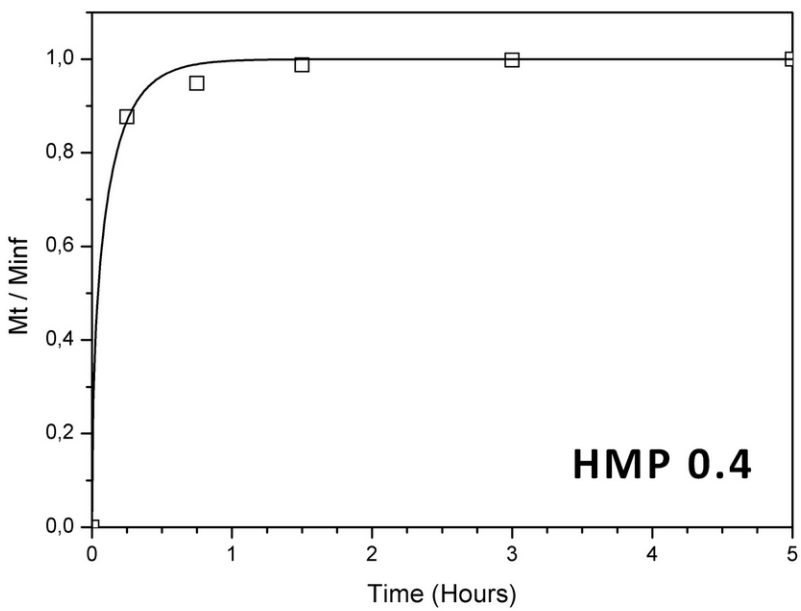
Mt / Minf
1,0
0,8
0,6
0,4
0,2
0,0
0
1
2
3
4
5
Time (Hours)
HMP 0.4

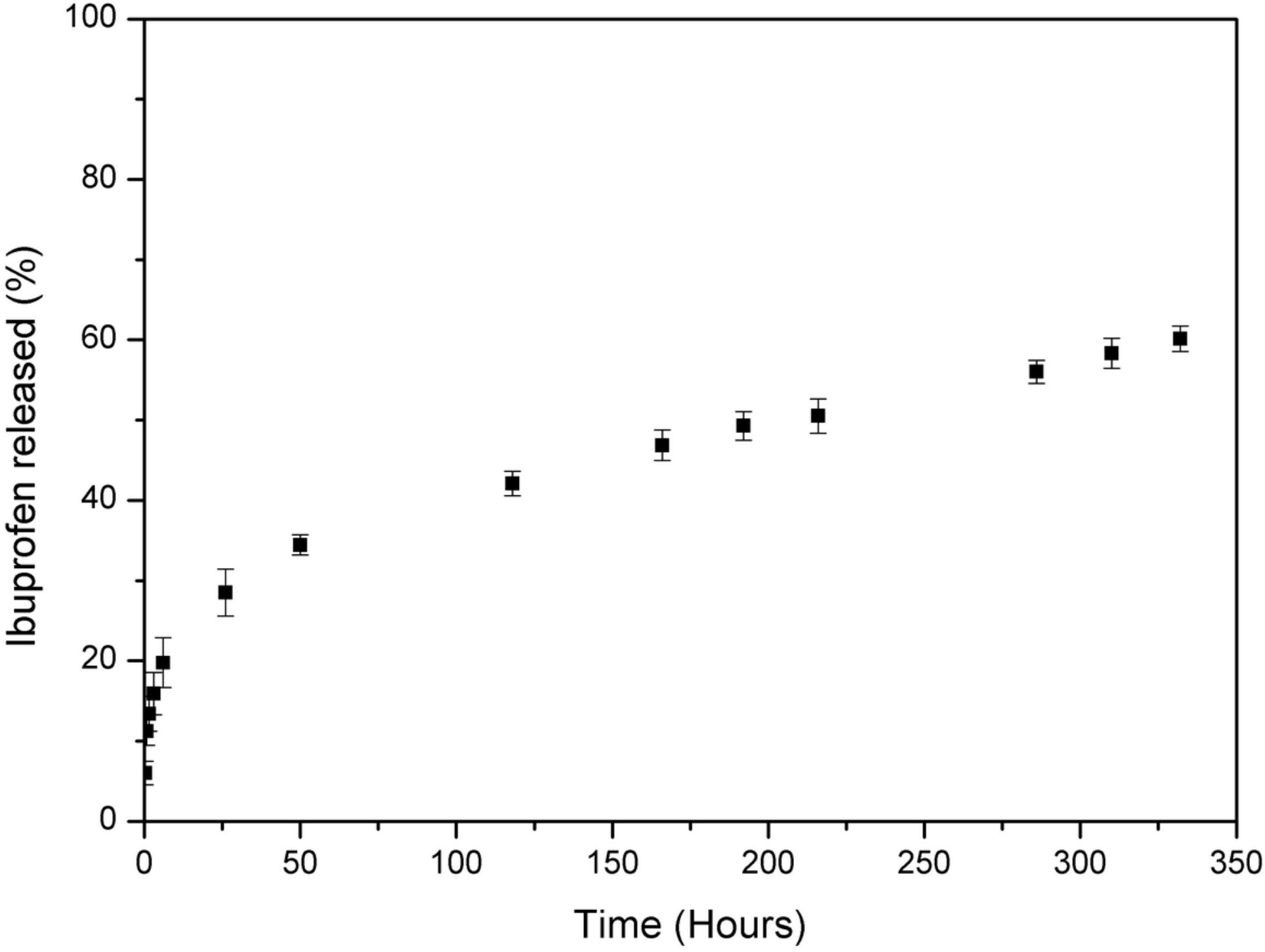
Ibuprofen released (%)
Time (Hours)
0
20
40
60
80
100
0
50
100
150
200
250
300
350

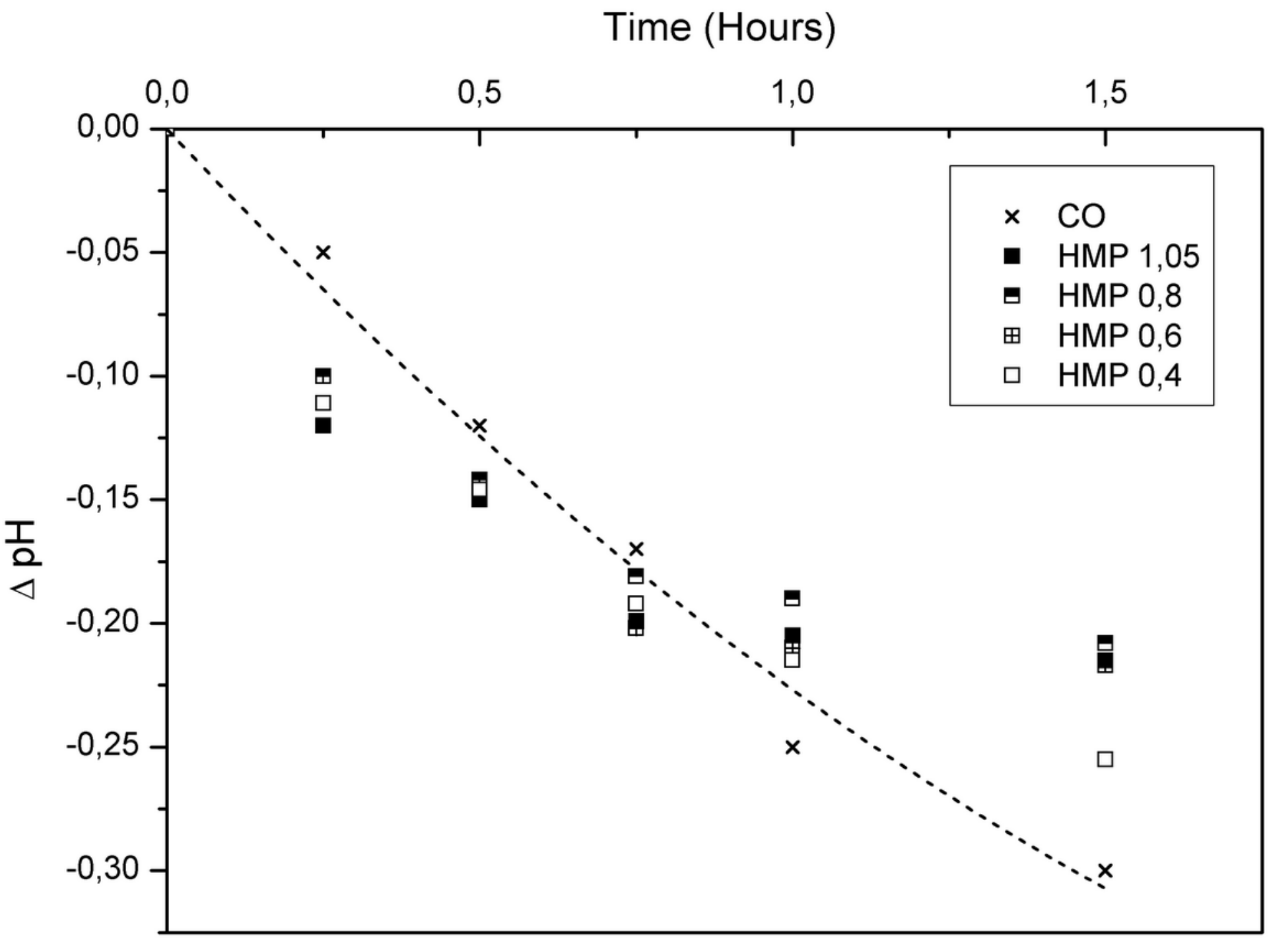
Time (Hours)
0,0
0,5
1,0
1,5
0,00
-0,05
-0,10
-0,15
-0,20
-0,25
-0,30
Δ pH
CO
HMP 1,05
HMP 0,8
HMP 0,6
HMP 0,4

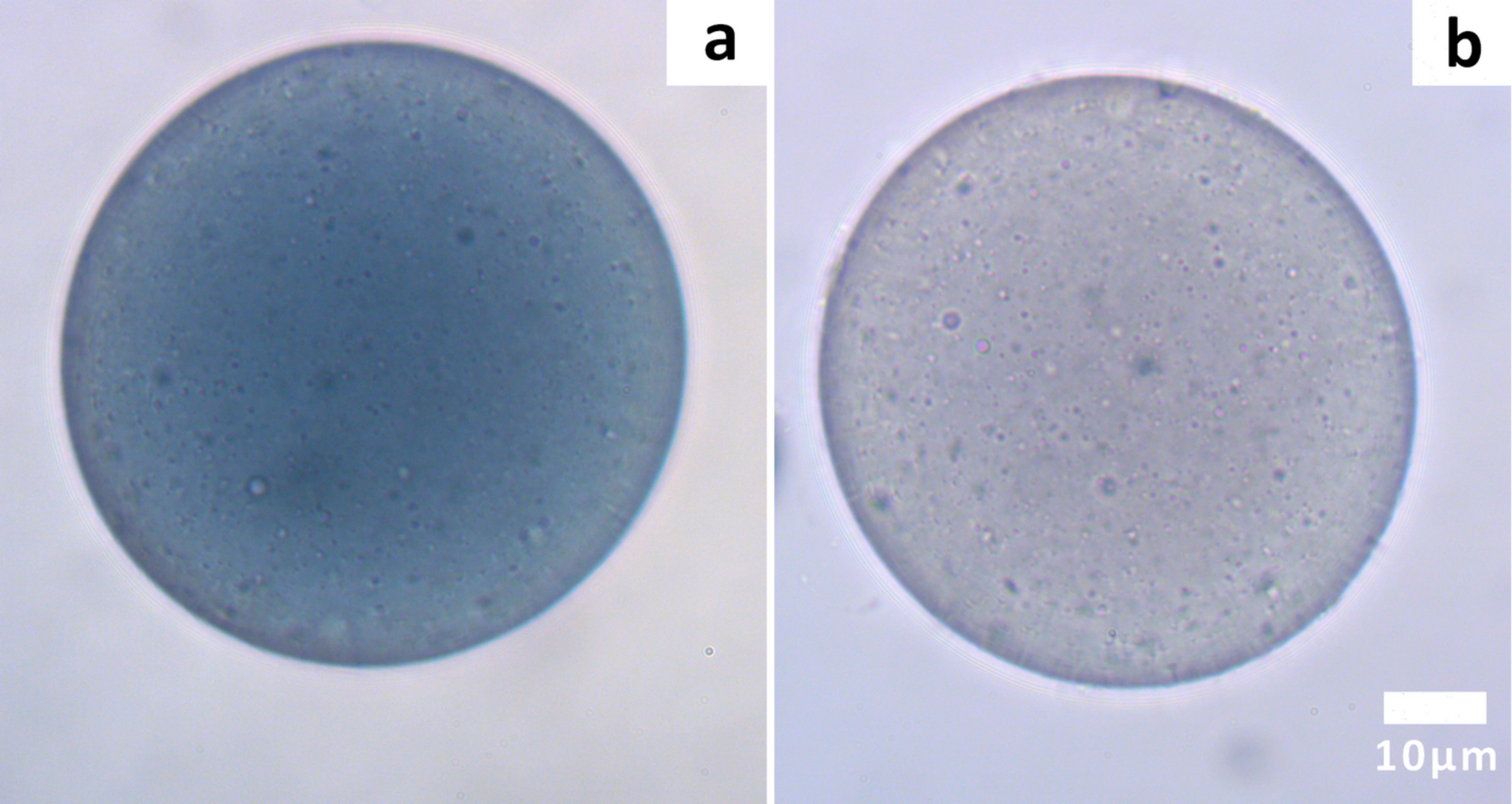
a
b
10µm

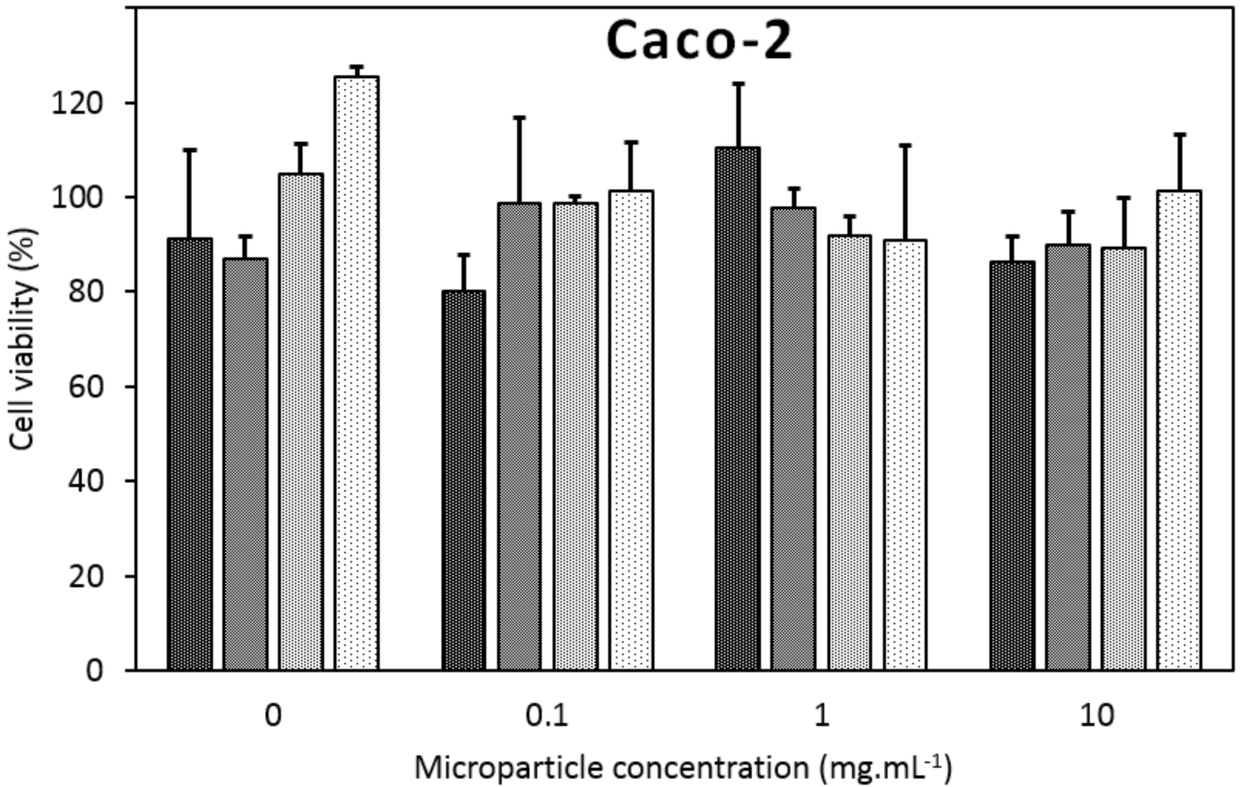
Caco-2
Cell viability (%)
0
20
40
60
80
100
120
0
0.1
1
10
Microparticle concentration (mg.mL-1)

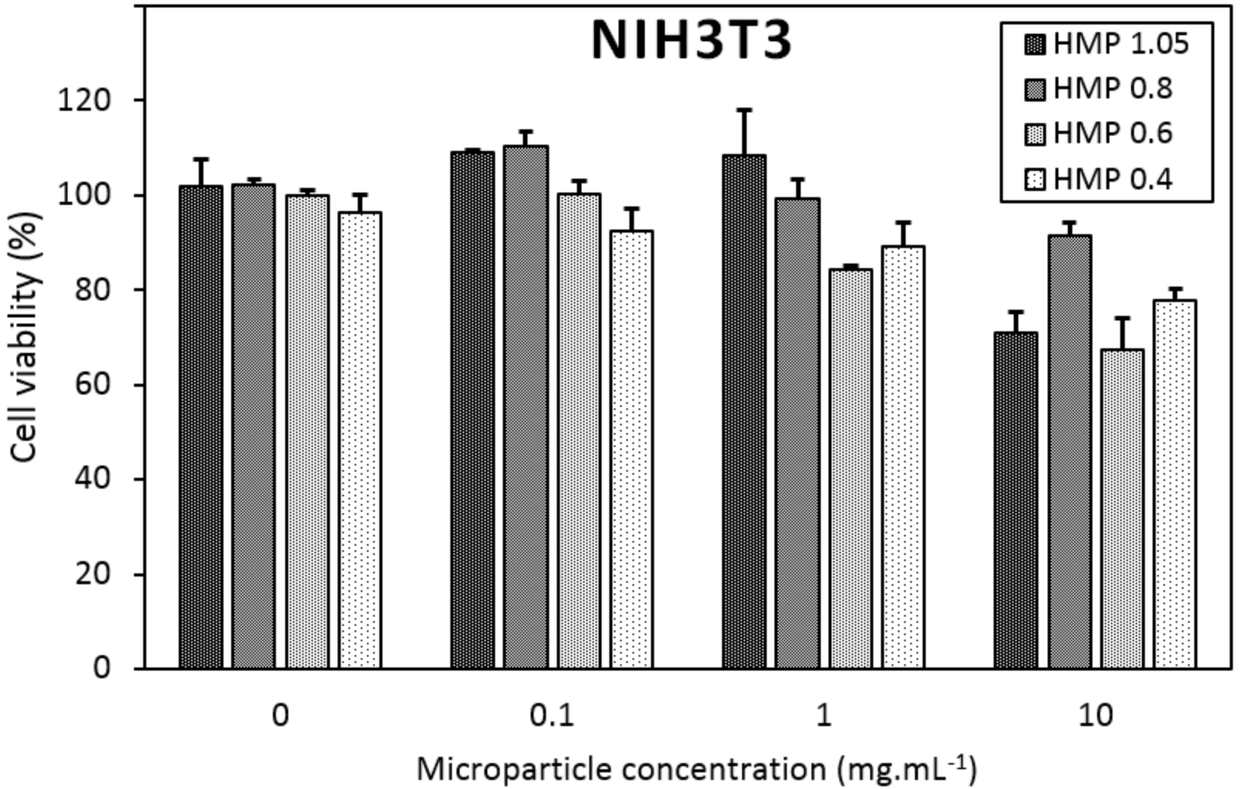
NIH3T3
HMP 1.05
HMP 0.8
HMP 0.6
HMP 0.4
Cell viability (%)
0
20
40
60
80
100
120
0
0.1
1
10
Microparticle concentration (mg.mL-1)

Table 1. Physicochemical properties of ICOs.

ICO	Molecular weight ($g \cdot mol^{-1}$)	Viscosity (mPa·s)	density
1.05	1600.9	961	0.999
0.8	1467.5	764	0.994
0.6	1334.1	709	0.986
0.4	1200.7	682	0.970
Castor oil	932.7	661	0.907

Table 2. Preparation yields of HMPs synthesized with the corresponding ICO. Data are shown as mean ± SD (n=3).

HMPs	Preparation yield η (%)	Weight loss by ethoxysilanes hydrolysis (%)	Corrected preparation yield η' (%)
1.05	73.4 ± 1.4	21.9	95.3 ± 1.4
0.8	70.0 ± 1.6	19.1	89.1 ± 1.6
0.6	75.3 ± 2.9	15.7	91.0 ± 2.9
0.4	75.7 ± 2.5	11.7	87.4 ± 2.5

Table 3. Volume Median Diameters (VMD)s, spans and deducted parameters (volume and surface area moment means) of HMPs wit four X_R. Data are shown as mean±SD (n=3).

HMP	VMD (µm)	Span	D [4,3] (µm)	D [3,2] (µm)
1.05	53.8 ± 4.9	1.38 ± 0.05	56.7 ± 5.1	22.3 ± 1.8
0.8	55.0 ± 5.3	1.55 ± 0.15	58.0 ± 5.3	22.4 ± 2.5
0.6	51.5 ± 2.7	1.67 ± 0.09	57.1 ± 6.9	19.9 ± 0.2
0.4	52.3 ±2.9	1.54 ± 0.11	54.9 ± 2.9	22.6 ± 1.0

Table 4. Condensation yields and degree of HMPs with various X_R.

HMPs [a]	^{29}Si signal (%)					CY (%)	CD (%)
	LP (-45 ppm)	T^0 (-48 ppm)	T^1 (-53 ppm)	T^2 (-57 ppm)	T^3 (-67 ppm)		
1.05	39.9	3.3	3.4	21.8	31.6	60.1	78.6
0.8	11.4	7.5	2.8	42.5	35.8	88.6	73.4
0.6	1.7	5.5	4.4	42.4	46.0	98.3	77.0

[a)]: HMPs 0.4 exhibited an insufficient signal-to-noise ratio to reach the confident accuracy of integrations (>95 %).

Table 5. Mass percentage of fluorine obtained from EDX spectra on a cross-section of 8 % flurbiprofen-loaded HMP. Data are shown as mean ± SD (n=3) and the technical accuracy was ±10 % of each value.

Spectrum	Atomic rate (%)		
	Fluorine	**Carbon**	**Silicium**
1	0.44 ± 0.2	81.9 ± 4.0	1.87 ± 0.9
1'	0.49 ± 0.1	81.3 ± 0.7	1.73 ± 0.7
2	0.45 ± 0.1	82.7 ± 2.0	1.52 ± 0.4
2'	0.37 ± 0.1	82.7 ± 0.5	2.16 ± 0.9
3	0.52 ± 0.1	81.6 ± 3.0	1.75 ± 0.9
3'	0.39 ± 0.0	80.8 ± 1.1	1.77 ± 0.6
4	0.42 ± 0.2	81.7 ± 2.7	1.68 ± 0.6

Table 6. Diffusion coefficients (D) deducted from the mathematical model. Results are shown as value ± probability of deviation

HMP	Diffusion coefficient (10^{-9} $cm^2.s^{-1}$)
1.05	1.44 ± 0.23
0.8	2.96 ± 0.18
0.6	4.35 ± 0.23
0.4	7.28 ± 0.75

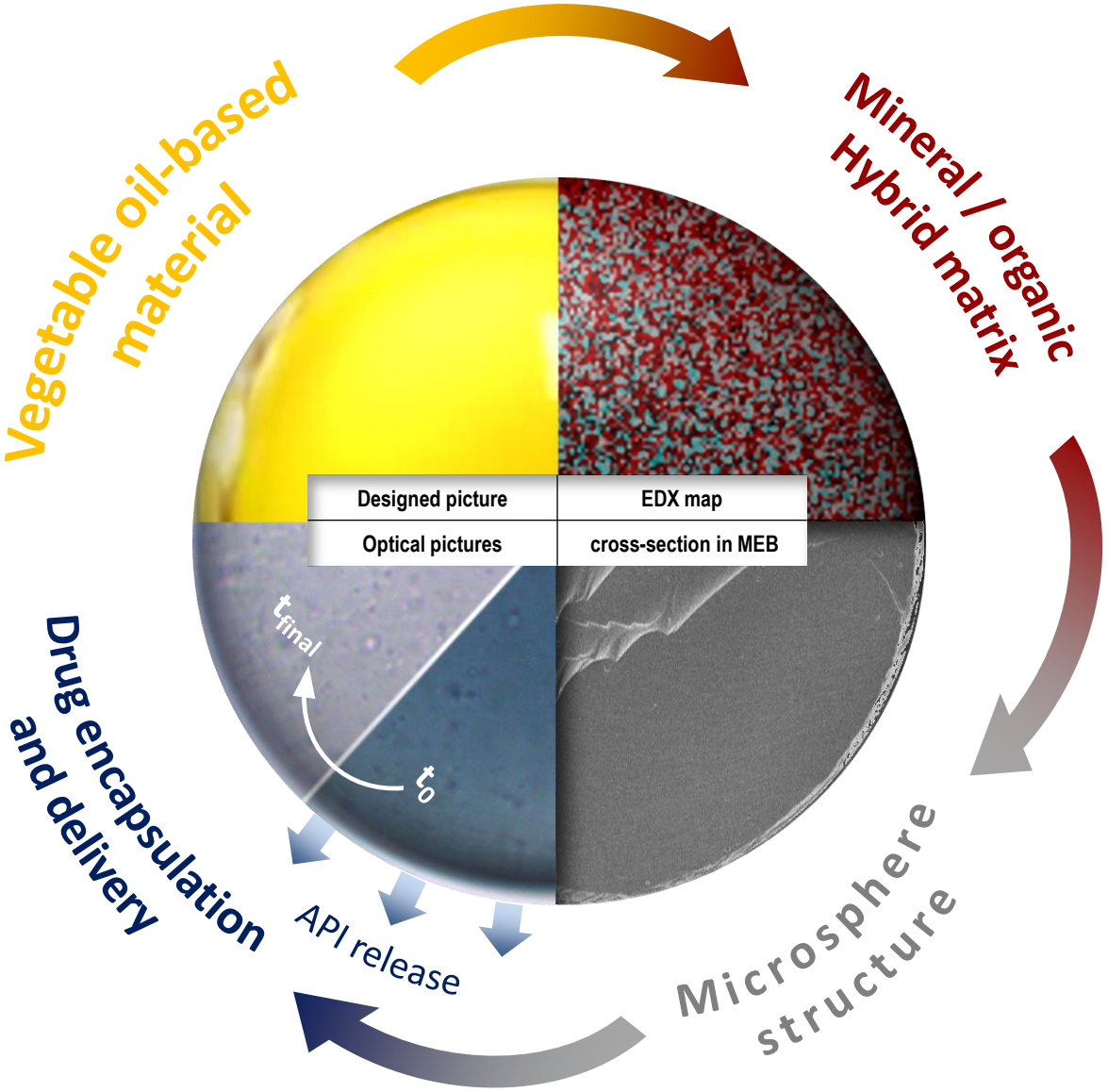
Vegetable oil-based material
Mineral / organic Hybrid matrix
Designed picture
EDX map
Optical pictures
cross-section in MEB
t_{final}
t_0
Drug encapsulation and delivery
API release
Microsphere structure